Functional magnetic resonance imaging in white matter using 3 T gradient-echo-planar imaging

by

Matthew James Courtemanche

B.Sc., Simon Fraser University, 2014

Thesis Submitted in Partial Fulfillment of the
Requirements for the Degree of
Master of Applied Science

in the
School of Mechatronic Systems Engineering
Faculty of Applied Science

SIMON FRASER UNIVERSITY
Fall 2016

Approval

Name:	**Matthew James Courtemanche**
Degree:	**Master of Applied Science**
Title:	***Functional magnetic resonance imaging in white matter using 3 T gradient-echo-planar imaging***
Examining Committee:	**Chair:** Kevin Oldknow Senior Lecturer

Carolyn Sparrey
Senior Supervisor
Associate Professor _____

Ryan D'Arcy
Supervisor
Professor _____

Alexander MacKay
Supervisor
Professor
Physics and Radiology
The University of British Columbia _____

Teresa Cheung
Internal Examiner
Professor of Professional Practice
School of Engineering Science
Simon Fraser University _____

Date Defended: December 14, 2016

Ethics Statement

The author, whose name appears on the title page of this work, has obtained, for the research described in this work, either:

a. human research ethics approval from the Simon Fraser University Office of Research Ethics,

or

b. advance approval of the animal care protocol from the University Animal Care Committee of Simon Fraser University;

or has conducted the research

c. as a co-investigator, collaborator or research assistant in a research project approved in advance,

or

d. as a member of a course approved in advance for minimal risk human research, by the Office of Research Ethics.

A copy of the approval letter has been filed at the Theses Office of the University Library at the time of submission of this thesis or project.

The original application for approval and letter of approval are filed with the relevant offices. Inquiries may be directed to those authorities.

Simon Fraser University Library
Burnaby, British Columbia, Canada

update Spring 2010

Abstract

White matter structures make up functional connectivity of the brain. The ability to observe white matter in action will provide insight into both normal brain function, as well as diseases characterized by loss of white matter integrity. Detection of functional magnetic resonance imaging (fMRI) activation in white matter is has been increasingly reported despite historically being controversial. The majority of development work to-date has used high-field MRI and specialized pulse sequences. In the current study, we utilized 3T MRI and a commonly applied gradient echo (GRE) echo-planar imaging (EPI) sequence to probe the robustness of fMRI activation using conventional clinical conditions. Functional activity was stimulated in target regions of interest within the corpus callosum, using an established visual-motor interhemispheric transfer task. The results confirmed that it was possible to detect white matter fMRI activation at the group level (N = 13, healthy individuals). Individual analyses revealed that 8 of the 13 individuals showed white matter activation in the body of the corpus callosum. Overall, the group results replicated prior 4 T MRI studies, but showed a lower percentage of individuals with activation. The findings support the concept that while white matter activation is detectable, the activation levels are close to thresholds used for routine 3 T MRI studies. Furthermore, by applying alternate hemodynamic response functions during analysis, larger clusters of activation were seen at the group-level.

Keywords: Functional magnetic resonance imaging; white matter; corpus callosum; hemodynamics

Acknowledgements

I would like to thank my committee for guiding me through this journey, as well as my colleagues at the NeuroSpine and NeuroTech labs for their support and comradery.

Table of Contents

Approval ii

Ethics Statement iii

Abstract iv

Acknowledgements v

Table of Contents vi

List of Tables viii

List of Figures ix

1 Introduction 1

1.1 Magnetic resonance imaging . . . 1

1.1.1 Nuclear magnetic resonance: physical principles . . . 1

1.1.2 Detection of nuclear magnetic resonance signal . . . 3

1.1.3 Magnetic resonance imaging: spatial discrimination within NMR . . . 5

1.1.4 k-space . . . 5

1.1.5 Pulse sequences . . . 6

1.1.6 Relaxation times . . . 9

1.1.7 Functional magnetic resonance imaging: blood oxygenation level dependent contrast . . . 10

1.1.8 Signal enhancement by extravascular protons . . . 11

1.1.9 Diffusion weighted imaging . . . 11

1.2 Analysis of functional MRI data . . . 12

1.2.1 Preprocessing . . . 12

1.2.2 Assessment using independent components analysis . . . 13

1.2.3 First-level or individual statistics . . . 13

1.2.4 Higher-level or group statistics . . . 15

1.3 Functional Neuroimaging of White Matter . . . 15
1.3.1 Connectivity model of the brain . . . 15
1.3.2 Role of white matter in plasticity . . . 16
1.3.3 Role of white matter in disease . . . 17
1.3.4 Investigations into BOLD fMRI in WM . . . 20

2 Confirmation of WM activity in fMRI using conventional GRE EPI sequences at 3 T 22
2.1 Background . . . 22
2.2 Methods . . . 24
2.2.1 Participants . . . 24
2.2.2 Experimental design . . . 24
2.2.3 MRI acquisition . . . 25
2.2.4 Functional MRI analysis . . . 25
2.3 Results . . . 27
2.3.1 Task compliance . . . 27
2.3.2 Group-level results . . . 27
2.3.3 Individual-level results . . . 29
2.4 Discussion . . . 31

3 Conclusion 33
3.1 Functional MRI in white matter . . . 33
3.2 Significance . . . 33
3.3 Future research directions . . . 34
3.3.1 In magnetic resonance imaging . . . 34
3.3.2 In magnetoencephalography . . . 34

Bibliography 36
References . . . 36

List of Tables

Table 1.1 Overview of recent MRI-based literature reporting WM integrity as a factor in disease pathology or progression 19

Table 2.1 FLOBS parameters for generating hemodynamic response function bases 26
Table 2.2 Featquery group-level results 29
Table 2.3 Individual-level percent signal change results 30

List of Figures

Figure 1.1 Spin precession in magnetic field 2
Figure 1.2 Zeeman splitting 3
Figure 1.3 Radio frequency pulse excitation 4
Figure 1.4 Slice selection in MRI 6
Figure 1.5 k-space plane 7
Figure 1.6 Spin-echo pulse diagram 8
Figure 1.7 Gradient-echo pulse diagram 8
Figure 1.8 k-space trajectories 9

Figure 2.1 Summary of results from previous studies WM fMRI studies 24
Figure 2.2 HRFs generated using FLOBS 26
Figure 2.3 Group level summary from HRF1 with threshold $Z > 2.0$ 28
Figure 2.4 HRF dependent group level activation 28
Figure 2.5 Individual-level activation 30

Chapter 1

Introduction

White matter is the tissue that forms the neural connections within the brain. Large effort has been put toward generating the human connectome, a map of all the brain's functional connections. While structural information is more readily obtainable, it is difficult to ascertain the functional aspects. In the healthy brain, white matter function has been successfully observed using highly specialized functional magnetic resonance imaging methods.

In addition to the typical phenomena in the healthy brain, there are longer time-scale dynamics which can occur. Learning new knowledge and skills modulates myelination, reinforcing neural pathways in a process known as plasticity. On the other hand, several diseases such as Alzheimer's disease and multiple sclerosis are characterized by deficits in white matter integrity. Reliable methods to quantitatively observe white matter function may provide new tools for the understanding and management of such diseases.

The objectives of this thesis are to:

1. Replicate fMRI activation in white matter achieved only with specialized conditions by using clinically accessible methods, namely gradient-echo-planar imaging sequences on a 3 T MRI system.

2. Improve sensitivity to white matter activation in fMRI analysis by investigating the effects of different hemodynamic response models, motivated by the difference in perfusion between white and gray matter.

1.1 Magnetic resonance imaging

1.1.1 Nuclear magnetic resonance: physical principles

Magnetic resonance imaging (MRI) is a non-invasive and powerful method of medical imaging in which proton spins are manipulated with the use of an external magnetic field to generate high resolution structural and functional images. When biological tissues con-

taining water and fat are subjected to the large, constant main magnetic field of an MRI scanner, the hydrogen atoms precess about the axis of the applied field (Figure 1.1).

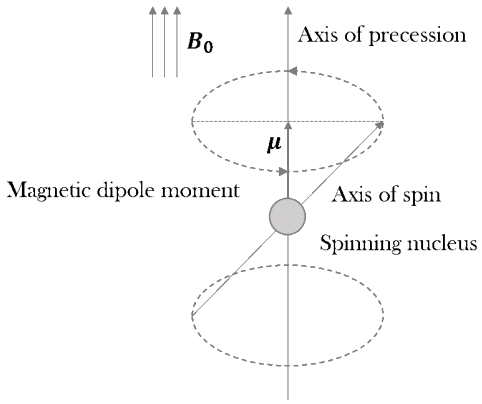

Figure 1.1: Precession is the rotation of the axis of a spinning body around another fixed axis due to torque. The upward magnetic field, $\boldsymbol{B}_0$, is the fixed axis, and also provides the torque when interacting with the spinning electron. Magnetic dipole moment $\boldsymbol{\mu}$ is proportional to the electron spin angular momentum.

This precession is the electromagnetic analogue of a gyroscope. The precessing nucleus has a magnetic moment, $\boldsymbol{\mu}$, by tracing an effective current loop through which it can interact with external magnetic flux. The angular precessional frequency is given by the Larmor equation,

$$\omega_0 = \gamma \boldsymbol{B}_0. \tag{1.1}$$

where ω_0 is the Larmor frequency, γ is a property of the target nucleus called the gyromagnetic ratio, and $\boldsymbol{B}_0$ is the magnitude of the main magnetic field (Larmor, 1897). In water protons, the value of γ is 42.6 MHz/T. In a 3 T field, the water protons precess at 127.8 MHz, which is in the VHF band, above the upper limit of FM radio range (108 MHz) (ITU-R, 2015). An atom in an external magnetic field gains energy from the interaction of its magnetic dipole moment with the field, $U_{Magnetic} = -\boldsymbol{\mu} \cdot \boldsymbol{B}_0$. Due to the Zeeman effect, a spinning nucleus in a magnetic field will split into two energetic states: parallel and anti-parallel to $\boldsymbol{B}_0$ (Zeeman, 1897). The quantum energy difference between states is given by $\Delta U_{Splitting} = \hbar\omega_0$, where $\hbar$ is Planck's constant (Figure 1.2).

Unlike a gyroscope which eventually decays towards the gravitational source, a spin is unable to align fully with the magnetic field due to the presence of thermal energy. Thermal energy is given by $U_{Thermal} = k_B T$, where k_B is Boltzmann's constant, and T is temperature. At physiological temperature, this energy is several orders of magnitude larger than the energy difference between the two precessional states available, or $\hbar\omega_0/k_B T \ll 1$. Given Boltzmann probability, the distribution of spins in parallel versus anti-parallel with $\boldsymbol{B}_0$ in a sample is determined by the spin excess,

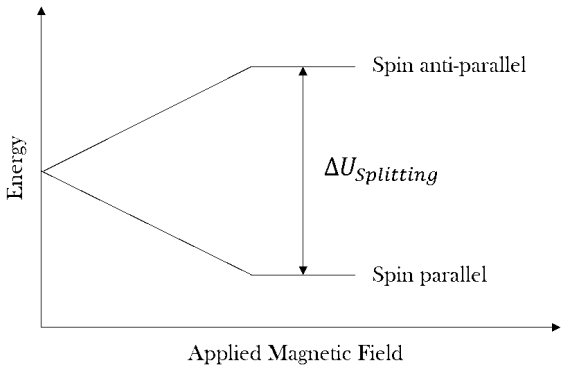

Figure 1.2: Zeeman splitting in the presence of magnetic field. Spinning atoms have quantized properties determined by their state. States are commonly described using quantum numbers $[n, \ell, m_\ell, m_s]$ for energy or principle quantum number, orbital angular momentum, orbital magnetic quantum number, and spin magnetic quantum number. By applying energy via an external field to a spinning atom, more states of m_ℓ become available, splitting the emission spectrum of the atom.

$$spin\,excess = N_{total}\frac{\hbar\omega_0}{2k_BT}. \tag{1.2}$$

where N_{total} is the number of spinning nuclei within the sample. While the number of protons giving rise to magnetic resonance signal is in the parts-per-million, it must be compared to the Avogadro quantities of atoms within a small region of tissue. Combining the spin excess (Equation 1.2), with the magnetic moment component of $\gamma\hbar/2$, the Larmor equation (Equation 1.1), and the spin density of sample ρ_0 results in the net longitudinal equilibrium magnetization,

$$M_0 = \rho_0\frac{\gamma^2\hbar^2}{4k_bT}B_0. \tag{1.3}$$

1.1.2 Detection of nuclear magnetic resonance signal

Bulk equilibrium magnetization does not produce a detectable signal on its own. The collection of spins must be perturbed away from the direction of $\boldsymbol{B}_0$ axis. This is accomplished by applying a radio frequency (RF) pulse, $\boldsymbol{B}_1$, orthogonal to $\boldsymbol{B}_0$, and centered at ω_0 using a transmitter coil. Microscopically, this will rotate $\boldsymbol{\mu}$ towards the transverse plane (Figure 1.3). Macroscopically, the material magnetization, M, is rotated into the transverse plane and begins to disperse. The angle through which the magnetization will rotate is known as the flip angle, and is determined by the integration of the amplitude and time of the RF pulse.

After the RF pulse is removed, the magnetization will return to equilibrium, releasing energy as magnetic flux. The time-varying magnetic flux induced by the rotating magne-

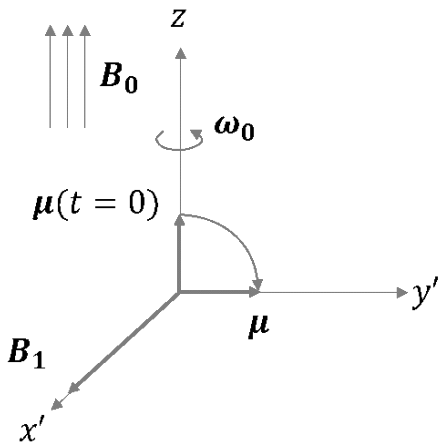

Figure 1.3: In the rotating ω_0 frame, at $t = 0$ the magnetic moment $\boldsymbol{\mu}$ is aligned with $\boldsymbol{B}_0$. Application of the RF pulse $\boldsymbol{B}_1$ causes $\boldsymbol{\mu}$ to rotate downwards into the transverse plane. In a frame rotating at the Larmor frequency, the magnetic moment appears stationary.

tization generates voltage in an inductively coupled receiver coil. From Faraday's law of induction, the induced voltage in the receiver coil can be written as

$$emf = -\frac{d}{dt}\int d^3r \boldsymbol{M}(\boldsymbol{r},t)\cdot\boldsymbol{\mathcal{B}}_{Reciever}(\boldsymbol{r}), \tag{1.4}$$

where $\boldsymbol{\mathcal{B}}_{Reciever}$ is a sensitivity factor of the receiver coil. From Equations 1.3 and 1.4, detected MR signal strength is proportional to the following properties:

$$signal \propto \rho_0\gamma^3 B_0^2 T^{-1} \tag{1.5}$$

By inspection of Equation 1.5, the following remarks can be made:

1. It is conceptually logical that higher spin density will yield stronger signal. Choice of target nucleus will be restricted by relative abundance in the sample.

2. Choice of spin nucleus is critical due to the cubic dependence on the gyromagnetic ratio.

3. From classical physics, $\gamma = 2\pi\frac{q}{2m}$, where q and m are the charge and mass of the body. Combining points 1 and 2, hydrogen atoms are an obvious choice of nucleus due to having both a large relative abundance in biological tissue as well as a large gyromagnetic ratio due to it being the lightest element.

4. It is evident that higher field strength will yield a quadratic increase in signal. Fortunately, background (off ω_0 resonance) signals exhibit a lesser dependence on field strength, which provides further separation for increased signal-to-noise.

1.1.3 Magnetic resonance imaging: spatial discrimination within NMR

In magnetic resonance imaging, the field of view or imaging volume is larger than the single sample region used in nuclear magnetic resonance (NMR) spectroscopy, and the key difference in methodology is the capability to resolve the spatial origin of subcomponents within the signal. There are methods to introduce spatial selectivity within the volume for excitement and measurement of signal. This is accomplished using magnetic gradients to apply spatial dependence to the magnetic field strength within the scanner bore. These gradients are created by pairs of additional magnetic coils within the scanner. In 3D, and in the presence of non-uniform magnetic field, the Larmor equation is modified accordingly,

$$\omega(\boldsymbol{r}) = \gamma[B_0 + G(\boldsymbol{r})]. \tag{1.6}$$

This principle can be extended into multiple dimensions by the addition of magnetic field gradients along different axes. Typically, this is used for slice selection as well as one in-plane axis, called the frequency-encoding axis. Discrimination of the third axis is achieved by pulsing another gradient temporarily to introduce a precessional phase gradient, known as the phase-encoding axis. By tuning the center frequency of the RF pulse, the middle of excited slice position can be chosen (Figure 1.4).

Recent studies have begun to explore applications of using multicoil arrays which can excite and recording multiple slices simultaneously (Larkman et al., 2001). This form of parallelization is referred to as multiband MRI, and it allows the acquisition time for a single volume to be reduced greatly (Moeller et al., 2010). This reduction in acquisition time of a sequence yields benefits of increased temporal resolution, reduced scan time, or increased signal-to-noise ratio (SNR), depending on the desired effect (Feinberg & Setsompop, 2013).

1.1.4 *k*-space

The decay signal after excitation is recorded with a receiving coil. This continuous signal will contain amplitude, frequency, and phase information which is the true form of MRI data. This analog signal is digitized and initially stored in k-space form. k-space is represented as a complex plane with orthogonal axes of frequency- and phase-encoding for typical 2D slice-wise scanning sequences (Figure 1.5).

Some sequences referred to as 3D sequences will correspond to digitizing data into a 3-dimensional k-space. The discrete elements of k-space are populated throughout the duration of the scan, along a trajectory determined by the pulse sequence. A real space image is generated from a populated k-space through the application of a 2D or 3D Fourier transform, corresponding to the k-space dimensionality. The size of k-space, its quantization upon digitization, will determine the resolution of the reconstructed image.

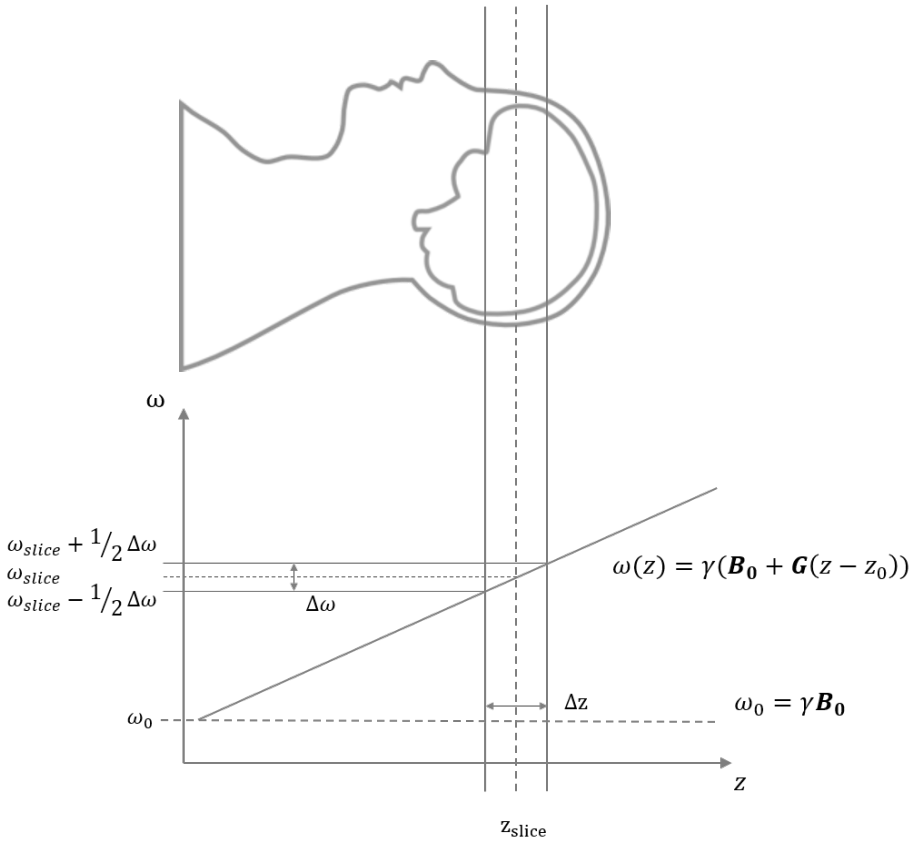

Figure 1.4: MRI slice selection for transverse acquisition. Superposed onto the main field $\boldsymbol{B}_0$, a gradient is $\boldsymbol{G}$ applied along the superior-inferior axis. Magnetic field becomes a function of z position along the axis. According to Equation 1.6, the z position of the slice is chosen by setting the RF pulse center frequency. Bandwidth $\Delta\omega$ of the pulse will determine how much of the gradient sloped region Δz will be excited by the pulse.

1.1.5 Pulse sequences

A pulse sequence is the synchronous control timing of the gradient amplifiers, transmitter amplifiers, and receiver electronics. For example, a simplified pulse sequence will first turn the RF pulse on, then off, and then instruct the receiver electronics to begin recording the decay signal. The sequence diagram will include the expected response of the magnetization. In realistic sequences, there will be channels controlling slice selection, frequency-encoding, and phase-encoding by precisely modulating the respective gradient amplifiers.

Sequences are described by how they manipulate target spins. Spin echo (SE) and gradient echo (GE) are the two main classes of sequences in structural and functional imaging. SE sequences will initially apply a RF pulse to tip the spins away from equilibrium. Following this RF pulse, one or more 180° echo RF pulses are applied to reverse the phase of the dephasing transverse magnetization which will subsequently regain coherence, known as an echo, at the echo time (TE) (Figure 1.6). This process is repeated in periods of

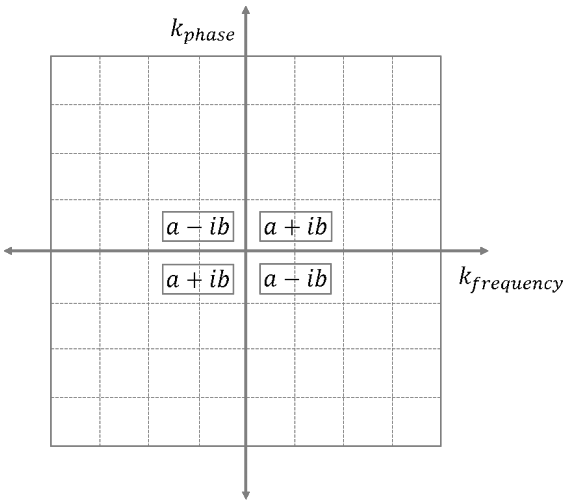

Figure 1.5: k-space represented in a complex plane with conjugate symmetry. The center of k-space contains low frequencies carrying bulk amplitude information. The periphery is populated by higher frequency information providing sharp edge definition in the finished image.

repetition time (TR). Gradient echo sequences apply a dephasing gradient during the initial decay forcing a more rapid dephasing of magnetization coherence, and then removing the dephasing gradient allowing coherence to return (Figure 1.7). This will produce an echo within the original decay envelope, without additional radio frequency energy deposition of additional pulses. Echo planar imaging (EPI) is a stepped application of phase switched gradient echoes, which allows for rapid collection of repeated echoes.

Pulse sequences are also described by their trajectory through k-space of an acquisition. Each line or segment within k-space is populated in a TR of the sequence. Cartesian traversal of k-space populates a row in each TR. Radial sampling populates k-space in a star-like pattern (Figure 1.8). Each TR of the sequence returns one spoke of the pattern. Advantages of radial sampling include: reduced burden of motion artifacts in the reconstructed image, reduced boundary aliasing due to the high frequency extents of the radial arms, and oversampling the low frequency center. Spiral methods begin at the origin of k-space and spirals outward. Spiral imaging has the advantages of reduced susceptibility field gradients leading to signal loss in EPI, and a faster traversal of k-space by ignoring the corners as compared to Cartesian sampling (Glover, 2012). Both spiral and radial methods are well behaved when undersampling in the form of compressed sensing or variable density sampling of k-space, which produce aliasing artifacts in reconstruction from Cartesian trajectories.

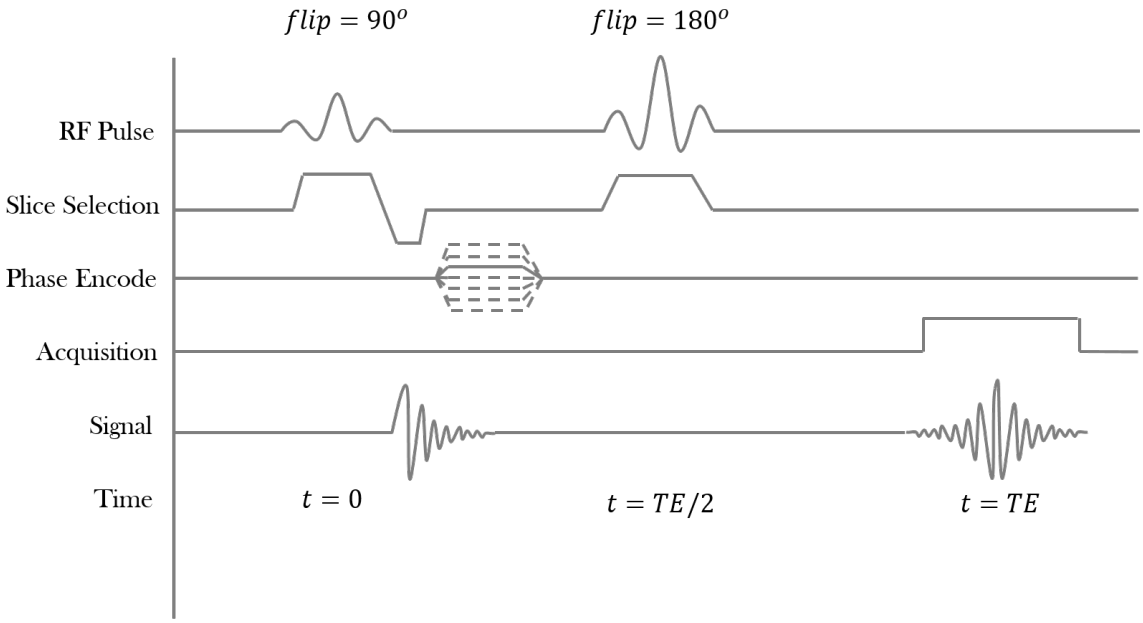

Figure 1.6: Simplified pulse sequence for spin echo readout. Within a single repeat time: a 90° RF pulse is issued while the slice selection gradient is active. The phase encoding gradient steps through levels in each TR. The excited signal will decay, and then be phase reversed and refocused by a 180° pulse. At echo time, TE, the signal will be recorded.

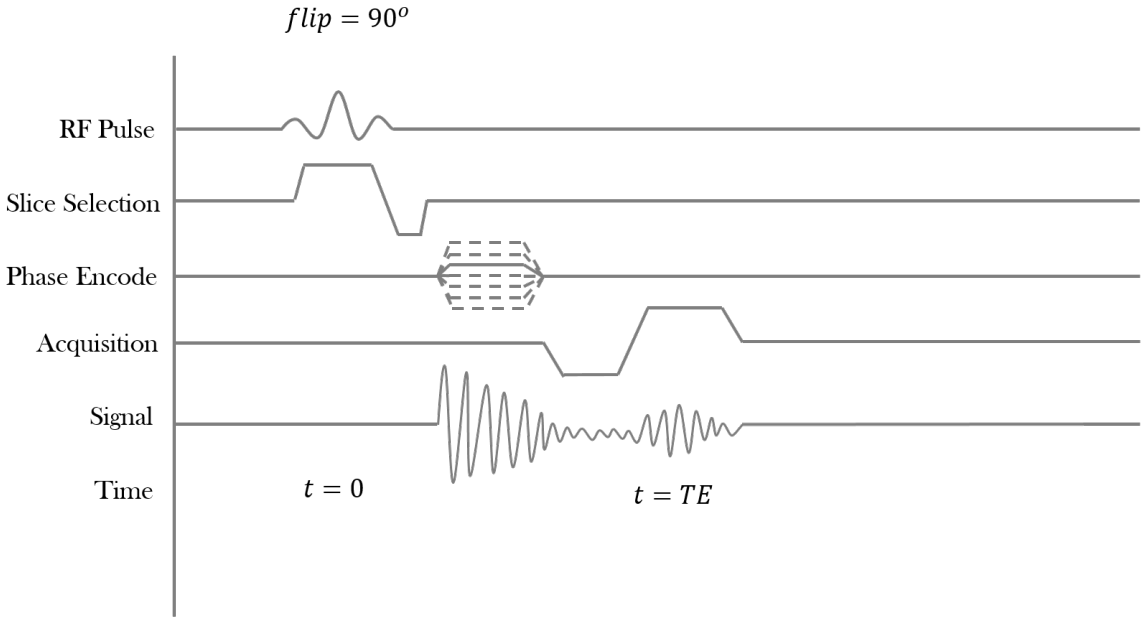

Figure 1.7: Simplified pulse sequence for gradient echo readout. Unlike spin echo, gradient echo sequences manipulate the coherence within the overall decay envelope. The signal is forced out of, then back into phase by applying a gradient. An echo is measured within the tail of the original T_2 decay time.

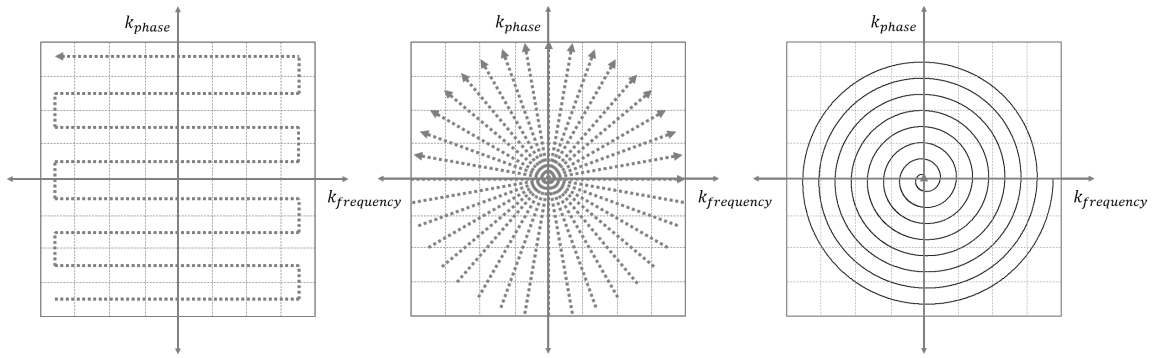

Figure 1.8: Typical k-space trajectories for Cartesian, radial, and spiral acquisition. Left: Cartesian sequences fix the phase-encode gradient while traversing the frequency axis. Center: Radial sequences populate k-space in "spokes" Right: Spiral sequences operate by driving the in plane gradients in a sinusoidal manner to spiral-in (shown) or spiral-out.

1.1.6 Relaxation times

MRI signal intensity is largely dependent on the number of nuclei within the volume, and sequences aimed to capture the concentration of hydrogen nuclei are known as proton density (PD) weighted. Within pulse sequence design, there is freedom to adjust TE and TR. There are multiple observable phenomena using MR imaging which can be selected for by adjusting these parameters. To illustrate this, the Bloch equations

$$\frac{dM_x(t)}{dt} = \gamma(\boldsymbol{M}(t) \times \boldsymbol{B}(t))_x - \frac{M_x(t)}{T_2} \tag{1.7}$$

$$\frac{dM_y(t)}{dt} = \gamma(\boldsymbol{M}(t) \times \boldsymbol{B}(t))_y - \frac{M_y(t)}{T_2} \tag{1.8}$$

$$\frac{dM_z(t)}{dt} = \gamma(\boldsymbol{M}(t) \times \boldsymbol{B}(t))_z - \frac{M_z(t) - M_0}{T_1} \tag{1.9}$$

can be solved and the individual relaxation phenomena examined (Bloch, 1946). Solving Equation 1.9 yields an exponential regrowth function with a time constant T_1,

$$M_z(t) = M_z(0)(1 - e^{-t/T_1}). \tag{1.10}$$

T_1, or spin-lattice relaxation, is a measure of magnetization returning to equilibrium along the main field after RF pulse. Sequences with short TE and TR will be T_1-weighted, and show higher intensity in fat. In the brain, fat is largely located in the myelin sheaths of white matter. Solving the first two of the separated Bloch equations gives an exponential decay function for transverse magnetization with characteristic time T_2,

$$M_{xy}(t) = M_{xy}(0)e^{-t/T_2} \tag{1.11}$$

T_2, or spin-spin relaxation, is a measure of phase coherence loss in the transverse plane as the individual spins precess at different rates. Sequences with long TR and TE will be T_2-weighted and highlight primarily water. However, T_2 is shortened by local field inhomogeneities and magnetic susceptibility effects (T_2'), causing more rapid coherence loss. The observed relaxation is denoted as T_2^*.

$$\frac{1}{T_2^*} = \frac{1}{T_2} + \frac{1}{T_2'} \tag{1.12}$$

When discussing magnetic fields in matter, as in tissue for this case, the notation changes. The material properties influence the functional aspects of a magnetic field in matter. Separating total current into bound and free terms in Ampère's law gives,

$$\frac{1}{\mu_0}(\nabla \times \boldsymbol{B}) = \boldsymbol{J} = \boldsymbol{J}_{bound} + \boldsymbol{J}_{free} = \boldsymbol{J}_{free} + (\nabla \times \boldsymbol{M}) \tag{1.13}$$

$$\nabla \times \boldsymbol{H} \equiv \nabla \times \left(\frac{1}{\mu_0}\boldsymbol{B} - \boldsymbol{M}\right) = \boldsymbol{J}_{free}. \tag{1.14}$$

The quantity $\boldsymbol{H}$ is often called the "magnetic field," while $\boldsymbol{B}$ is referred to as "flux density" or "magnetic induction." Examining Equation 1.14, and material specific magnetic permeability,

$$\chi_m = \frac{\mu}{\mu_0} - 1, \tag{1.15}$$

it is apparent that the magnetization response to the applied field is modified by this magnetic susceptibility,

$$\boldsymbol{B} = \mu_0(\boldsymbol{M} + \boldsymbol{H}) = \mu_0(1 + \chi_m)\boldsymbol{H}. \tag{1.16}$$

$$\boldsymbol{M} = \chi_m \boldsymbol{H}. \tag{1.17}$$

The physics of NMR and MRI are summarized in Equation 1.17. In MRI external magnetic fields $\boldsymbol{H}$ are applied which translate to magnetization $\boldsymbol{M}$ inside the tissue. Decay of magnetization signal is measured, and local variations in magnetic susceptibility χ_m give rise to image contrast via differences in measured magnetization relaxation times.

1.1.7 Functional magnetic resonance imaging: blood oxygenation level dependent contrast

First observed by Ogawa and colleagues, it was postulated that MR pulse sequences at a rapid TR can be applied to capture physiological dynamics (Ogawa, Lee, Kay, & Tank, 1990). Neurons require additional metabolic resources for sustained activity, and this is provided by increased blood flow. Blood carries oxygenated (diamagnetic) and deoxygenated (paramagnetic) hemoglobin. Blood oxygenation level dependent (BOLD) imaging operates on the principle that increased neurological demand will be met with an oversupply of oxyhemoglobin. This influx of paramagnetic species into the excited region will cause a change

in magnetic susceptibility χ_m giving rise to retention of signal in T_2^*-weighted sequences resulting in an increase of signal approximated in Equation 1.18 (Menon, Ogawa, Tank, & Ugurbil, 1993),

$$\frac{\Delta S}{S} = e^{-TE\Delta(1/T_2^*)} - 1 \cong -TE\Delta\left(\frac{1}{T_2^*}\right), \tag{1.18}$$

where, $\Delta S/S$ is the fractional change in signal. Repeatedly measuring this signal provides 4D data which can be statistically analyzed for activity when compared to an experimental paradigm. This principle has been the foundation of functional MRI using largely T_2^*-weighted GRE-EPI sequences since inception (Logothetis & Wandell, 2004).

1.1.8 Signal enhancement by extravascular protons

In addition to BOLD fMRI, another contrast mechanism operates on the basis of proton density changes, called signal enhancement by extravascular protons (SEEP) (Figley, Leitch, & Stroman, 2010). This method measures signal with contributions from both intra- and extravascular fluid (Stroman, Krause, Malisza, Frankenstein, & Tomanek, 2002). According to the balloon model of brain activation, not only does blood flow increase in active neuronal tissue, but cellular swelling due to an inrush of fluid also occurs in the neurons and glial cells, primarily astrocytes (Buxton, Wong, & Frank, 1998). This newer contrast mechanism is not yet widely studied or accepted (Jochimsen, Norris, & Möller, 2005). PD SE sequences can be designed to be sensitive to these changes, and this method has been applied with success in functional imaging of the spinal cord (Zhong et al., 2016).

1.1.9 Diffusion weighted imaging

In addition to the aforementioned methods of magnetic resonance imaging, the same apparatus can be used to measure the motion of water *in vivo*. Anisotropically restricted diffusion (ARD) was first proposed by Hajnal et al. in 1991 wherein the probability of diffusion is related to an echo intensity attenuation factor (Hajnal et al., 1991). Diffusion weighted imaging (DWI) involves the use of pulsed opposing non-uniform gradient fields which dephase and subsequently rephase water protons. Slow moving protons will experience a near-reciprocal field and return close to their original phase, whereas fast diffusing protons will experience a larger differential in opposed gradient and rephrase less, creating signal loss. The resulting signal of the voxel will be dominated by the concentration of slow moving water (Stejskal & Tanner, 1965). Diffusion tensor imaging (DTI) is the repeated application of this process in multiple directions of diffusion gradients and determines the diffusion tensor at each voxel (Moseley et al., 1990). The anisotropy of a diffusion tensor is indicative of the tissue structure imposing constraints on the free water molecules. The principle direction of diffusion has been used to construct structure maps of the myelinated

white matter tracts in the brain using DTI tractography (Douek, Turner, Pekar, Patronas, & Le Bihan, 1991).

1.2 Analysis of functional MRI data

The following steps for the analysis of fMRI data are implemented in multiple software packages including FSL (Jenkinson, Beckmann, Behrens, Woolrich, & Smith, 2012) and SPM , and may appear in different order or by different names, but in general achieve the same ends.

1.2.1 Preprocessing

Before fMRI statistics can be computed from data, several stages of processing must be applied in order to make the successive steps valid in their assumptions and methods.

1. *Cropping to the temporal region of interest.* Excess time volumes before or after the experimental task can be cropped to simplify definitions in the statistical model and to increase computational efficiency by reducing CPU cycle and memory usage.

2. *Motion correction.* Even while instructed to remain still in the scanner bed, and while constrained by the MR coils, participants will exhibit motion from both gross bodily movements as well as physiological processes such as breathing and cardiac pumping. Functional activation statistics are calculated using a grid of voxels quantizing the volume. Uncorrected motion would result in different samples of tissue passing in and out of a voxel across the duration of the experiment, which induces undue variance into the signal. Gross motion can be corrected by applying a registration to each volume of the data, optimizing the alignment between time points. Respiratory and cardiac motion can be mitigated using gating or breath hold techniques, but these are not practical for extended functional task experiments. Residual motion and physiological artefacts can be assessed using an independent components analysis following preprocessing.

3. *EPI fieldmap correction.* Images generated from EPI sequences are prone to distortion in regions of steep magnetic susceptibility gradients which mostly occur at tissue boundaries. This is primarily observed in the frontal lobe, superior to the orbit. Collecting a fieldmap during the MRI session will allow the EPI fMRI data to be spatially unwarped, but will not recover any lost BOLD signal. This will assist in registration of the EPI data to a structural image.

4. *Slice timing correction.* EPI sequences read out signals a single slice at a time. Within a TR, each slice will have an offset acquisition time as specified by the slice ordering of the collection protocol. Using information about the TR and the slice order, an

interpolated temporal shift can be applied to each slice of functional data. This will ensure that functional data will be temporally aligned to the experimental model throughout the volume.

5. *Brain extraction.* Registration to standard space or multi-modal images can be hindered by MRI's inclusion of extraneous anatomical structures. Additionally, removing non-brain voxels from the image reduces CPU and memory usage in subsequent stages of analysis.

6. *Spatial filtering.* Application of a 3D Gaussian kernel improves SNR by decreasing noise and increasing the normality of noise distribution, which will be required for subsequent processing. However, this low pass filtering comes at the cost of reduced resolution, added boundary artefacts, shifting of activation peaks, merging of nearby distinct clusters, and deletion of small clusters. Additionally, blurring individual results may yield stronger statistical results at the group level by reducing individual subject variability.

7. *Temporal filtering.* High-pass filtering in the time dimension is used in fMRI to reduce baseline variation and drift throughout the dataset. This will also shift the signal mean to near zero, which is needed for general linear model analysis.

1.2.2 Assessment using independent components analysis

Independent components analysis (ICA), linear in the case of fMRI analysis, is a method to decompose a signal into a linear combination of components at each voxel. In 4D fMRI data, these components are time-varying subsignals coupled with spatial volumes of coefficients (McKeown et al., 1998). Performing ICA on fMRI data can be done prior to preprocessing to assess the quality of the data, and after preprocessing to verify the results of critical steps such as motion correction. A typical ICA of fMRI will return on the order of 100 components. Ideally, these components will have separated out various phenomena including task-related signal change, motion or motion residual, and physiological effects such as fluid movement in the sinuses and ventricles. When performing model-based analyses, residual motion and physiological artifacts can be left in place, selectively filtered out of the data, or forwarded to the model as confounds.

1.2.3 First-level or individual statistics

For model-based analyses using multiple regressions, a general linear model (GLM) is constructed. Each voxel is represented by a linear combination of modelled response predictors, plus residuals. The following assumptions on the data are required for a GLM to be successful and valid:

1. The expectation value of the residuals must be zero,

$$E[\epsilon_i] = 0. \tag{1.19}$$

2. The residuals have constant variance,

$$Var[\epsilon_i] = \sigma^2 = constant. \tag{1.20}$$

3. All residuals are random and independent or uncorrelated,

$$Cov(\epsilon_i, \epsilon_j) = 0 \forall i \neq j. \tag{1.21}$$

4. Residuals are distributed normally,

$$\epsilon_i \sim N(0, \sigma^2). \tag{1.22}$$

These conditions are the assumption of whiteness, meaning that the error has constant power spectral density. While fMRI data are not necessarily in agreement with these assumptions even after preprocessing, pre-whitening algorithms can be applied prior to statistics.

A predictor is a vector containing an expected signal, and is the same length as the number of fMRI volumes. Each predictor in the model is a convolution of the experimental timing with a hemodynamic response curve. Each independent experimental condition will require its own predictor. A design matrix is the concatenation of all predictor vectors. Predictors should be temporally filtered using the same kernel as the data. Temporal derivatives of the main predictors can be added to the design matrix to allow for small temporal offsets that may be present in some voxels. In addition to experimental predictors, other variables can be added to the design matrix, such as motion confounds or ICA components. The GLM method attempts to fit the data as:

$$\boldsymbol{S}_i = PE_0 + \sum_{j=1}^{J} PE_j \boldsymbol{Pr}_{ij} + \boldsymbol{\epsilon}_i, \tag{1.23}$$

where $\boldsymbol{S}_i$ is the observed signal at the i^{th} voxel, PE_0 is a factor for accommodating a nonzero baseline (or equivalently a constant value predictor), PE_j are the parameter estimates or coefficients of the linear predictors $\boldsymbol{Pr}_{ij}$, and $\boldsymbol{\epsilon}_i$ is the residual, in a model with J predictors. Converting this equation to matrix form indicates that the vector of parameter estimates, $\boldsymbol{PE}$, can be solved in the presence of a generally non-invertible design matrix, $\boldsymbol{Pr}$, using algorithms of matrix algebra:

$$\boldsymbol{PrPE} = (\boldsymbol{S}_i - \boldsymbol{\epsilon}_i). \tag{1.24}$$

Contrast of parameter estimates (COPE) are linear combinations of interest of PEs from the design matrix, ie.

$$contrast\,[i\,j] : COPE = i \times PE_1 + j \times PE_2. \tag{1.25}$$

COPEs are used in determining the probability that the signal from a voxel is correlated with some combination of modeled predictors. A t-statistic is found as

$$t = \frac{COPE}{stdev(COPE)} \tag{1.26}$$

Here the necessity of whiteness of the data is apparent. It is assumed that COPEs are Student's t-distributed, and the null hypothesis is that COPE = 0. Using a t-score the t-distribution, the probability, and Z-score can be determined. In addition to contrasts, F-tests check for significant power contained within a combination of COPEs.

For making comparisons or combining the results from multiple participants, results of individual level statistics are transformed first to the individual's anatomical space and then to a standard space brain, often MNI152 (Evans et al., 1993). These transformations can be achieved using linear or non-linear means.

1.2.4 Higher-level or group statistics

Individual results can be combined using fixed- or mixed-effects statistics. Fixed-effects statistics describe only the members included in the input, and essentially creates a mean COPE for the group with uncertainties derived only from individual variances (VARCOPEs). Mixed-effects statistics attempts to produce a mean COPE describing the generalized population from which the specific individuals were drawn by using the distribution of individual COPEs to derive variance.

Results from multiple sessions of the same participant are combined using fixed-effects statistics. Groups of multiple participants, either single session or combined sessions, are then combined using mixed-effects statistics. These group statistics can be used to investigate questions such as, does a group exhibit a certain activity on average, or, is there a difference in activity between groups.

1.3 Functional Neuroimaging of White Matter

1.3.1 Connectivity model of the brain

The brain is divided into two roughly equal parts, white matter and gray matter (Black, 2007). White matter is largely comprised of neuronal axons, whereas the gray matter is the

soma and dendrites. As a graph, gray matter represents nodes and white matter the connecting edges. This white matter connectivity model originates from disconnection studies in which the corpus callosum, the anterior commissure, and the hippocampal commissures were transected in the attempted treatment of TBI-induced convulsions (Bogen & Vogel, 1962; Gazzaniga, Bogen, & Sperry, 1965; Geschwind, 1965). Split brain patients showed indication of visual hemispatial neglect and laterally selective verbal processing impairments. Reaction time studies in healthy individuals using visuo-motor crossed/uncrossed tasks established that normal brain processes involve interhemispheric transfer (IHT) (Marzi et al., 1999). Mathematical studies have begun to map the networks of the brain in order to understand the modular recruitment of processing centers for differing tasks as well as the interconnecting hubs, and their correlations with genetics and behaviour (He & Evans, 2010). A review of behavioural studies in the presence of white matter lesions illustrates that white matter is critical for connecting gray matter to facilitate complex neurological processing, and has expanded more in evolution than gray matter (Filley & Fields, 2016). In furthering the connectivity model for understanding brain function, it is critical to be able to interrogate white matter function.

1.3.2 Role of white matter in plasticity

In normal development, the human brain undergoes growth in white matter structure allowing for enormous complexity. The myelinated tracts interconnecting the gray matter cortex continually develop into the third decade of age (Giedd, 2004). This growth, or plasticity, can take the form of new structural synaptic connections, the modulation of myelination in existing axons, and the modulation of signal intensity in existing synapses. Plasticity can occur in normal development, as reaction or adaptation to stimulus exposure, briefly or extended, and to repair damage (Trojan & Pokorný, 1999).

Positive changes in brain activity attributed to plasticity can be observed in functional neuroimaging studies. Learning of complex skills such as piano playing is associated with observable changes in white matter organization, known as myelin plasticity. Structural complexity is proportional to time spent developing the skill (Bengtsson et al., 2005). Another study using jugglers indicates similar results (Scholz, Klein, Behrens, & Johansen-Berg, 2009). Even less complex tasks, such as auditory tone discrimination can produce an observable difference in fMRI after brief training (Jäncke, Gaab, Wüstenberg, Scheich, & Heinze, 2001).

Reorganization of brain connectivity can also occur, indicating the capacity for much larger scale changes in white matter. In relapsing-remitting multiple sclerosis, an increase in functional connectivity is noted in the acute phase of relapse as the brain compensates for a network with a new lesion burden (Droby et al., 2015). Additionally, over time the brain is able to adapt for absent senses, a review of studies suggests, as patients with unilateral hearing loss indicate bilateral functional activation to auditory stimulus in regions associ-

ated with auditory processing as well as other non-auditory regions (Heggdal, Brännström, Aarstad, Vassbotn, & Specht, 2016). In the developing brain of children with hemispherectomy, bilateral motor and sensory function were transferred to the remaining hemisphere, in a region outside the existing sensorimotor centers (Graveline, Mikulis, Crawley, & Hwang, 1998). In the adult brain, recovery of function and functional activation has been reported in the case of open head TBI involving loss of cortical tissue (D'Arcy et al., 2015).

1.3.3 Role of white matter in disease

Several disorders of the brain are associated with white matter integrity in its distributed systems. The roles that white matter plays are various, either in early pathogenesis where it can be an indicator of new disease onset, or as subject to a primary mechanism of degeneration leading to cognitive or physical deficits. A summary of selected studies indicating the pathogenic role of white matter abnormality in common neurological disorders is presented in (Table 1.1). Some comments on the contents of the table, noting changes in fractional anisotropy (FA) (measure of directedness in diffusion tensor) and mean diffusivity (MD) (average diffusion across all dimensions in diffusion tensor) are typical indicators of WM integrity in the presence of normal appearing WM (NAWM) in structural imaging. WM disruption may not be visually apparent and therefore missed in clinical scans. Most of the observations in Table 1.1 structural measures of WM, without any functional insight. Functional activity could be a missing piece, just as with diffusion, in order to understand hidden damage or disorder in NAWM.

Disorder	**Study**	**Findings**
Alzheimer's Disease (AD)	Dawe et al., 2016	Differentiating normal aging induced cognitive changes with cognitive decline, dementia, and AD via post-mortem MRI indicated largest observable differences in white matter integrity
	Habes et al., 2016	MRI WM hyperintensity (WMH) burden in AD changes indicate a significant association between AD, WMH, and cognitive decline beyond normal age related patterns.
	Gordon et al., 2015	Periventricular and deep WMH in MRI discriminate between healthy control and cognitively demented individuals. Amyloid deposition in WM is a predictor of cognitive decline.
	Taylor et al., 2016	WMH burden associated with decreased functional connectivity, and is an additional factor in AD development.

Multiple sclerosis (MS)	Wang et al., 2016	WM is vulnerable to ischemia and often damaged during ischemic stroke, leading to more likelihood of stroke and neurological issues including cognitive, emotional, sensorimotor impairment.
	Lassmann, 2014	MS is a demyelinating disease that exemplifies how damage to WM pathology can have devastating effect on all functions of the brain.
	Paul, 2016	Cognitive impairment in MS is linked to diffuse WM in MR images.
Traumatic brain injury (TBI) or mild traumatic brain injury (mTBI)	Alhilali et al., 2015	Patients suffering from mTBI or depression expressed decreased FA in the superior longitudinal fasciculus, nucleus accumbens WM, anterior limb of the internal capsule, and the cerebellar vermis.
	Armstrong et al., 2016	TBI can lead to irreversible damage in the form of demyelination and poor clinical outcomes.
	Astafiev et al., 2015	Concussion or mTBI can lead to persistent behavioral symptoms or impairment. Abnormal BOLD signals can reliably be detected in these patient groups years post TBI, even in structures appearing normal in MRI and DTI.
Dementia	Jung et al., 2014	In dementia of the Binswanger type, in addition to cortical atrophy, evidence of decreased WM integrity with reduced FA, high MD is present in the genu and splenium of corpus callosum.
	Kim et al., 2015	Periventricular WM hyperintensities (WMH) predicted all-cause dementia and dementia differentially by region and severity. Suggests WM integrity loss to be part of pathogenesis mechanism.
	Love & Miners, 2015	White matter abnormalities predict cognitive decline.
	Mahoney et al., 2014	In phenocopy and behavioural variant frontotemporal dementia white matter changes extend beyond localized gray matter atrophy.
	Meijboom et al., 2016	Phenocopy frontotemporal dementia is characterized by disruptions to WM microstructure.

Vanishing white matter disease (VWMD)	Pronk et al., 2006	Leukoencephalopathy with vanishing white matter is a genetic brain disorder. WM degenerates and is replaced by fluid as told by MRI and MRS
	Bugiani et al., 2010	Leukoencephalopathy with vanishing white matter is a poorly understood heritable disease characterized by rarefaction of WM.
Schizophrenia	Caprihan et al., 2015	Cognition in schizophrenia had no correlation with FA.
	Zhang et al., 2016	Widespread disruption of WM integrity occurs during early onset of schizophrenia
Creutzfeldt-Jakob disease (CJD)	Armstrong 2010	Variant CJD is marked by degeneration of cortical white matter where disease form prion protein induces axonal leakage.
	Caverzasi et al., 2014	Sporadic CJD is characterized by reduced MD in WM indicating a possible involvement in pathogenesis.
	Lee et al., 2012	Significant reductions of FA in CJD, associated severity with disease duration. Increase of radial diffusivity suggests axonal leakage.
	Matsusue et al., 2004	Cerebral WM lesions are a primary presentation of the pancephalopathic type CJD.
All-cause mortality	Sedaghat et al., 2016	Hazard ratio increase of all-cause and especially cardiovascular related deaths increase with decreased FA and increase MD.

Table 1.1: Overview of recent MRI-based (utilizing structural MRI, DTI, or fMRI) literature reporting WM integrity as a factor in disease pathology or progression. A common theme across these conditions is the disruption of WM structure and decrease in FA corresponding to lost WM integrity.

This survey of evidence indicates the importance of structure and integrity of white matter in the brain, and provides the motivation for its continued study using functional means. Furthermore, it illustrates the imperative to develop optimized techniques to be able to quantitatively detect functional activation in WM because structural means in some cases provide no insight. While the studies in Table 1.1 specifically focus on structural MRI and DWI measures to infer the functional status of WM, they do not observe it directly. Developing and employing reliable fMRI methods in WM will provide additional metabolic information, which along with structural and diffusion data can provide a more complete picture of pathologies in WM.

1.3.4 Investigations into BOLD fMRI in WM

While it has been successfully demonstrated, imaging functional activation of white matter using the BOLD contrast remains challenging (Gawryluk, Mazerolle, & D'Arcy, 2014). BOLD signal depends on both cerebral blood volume and cerebral blood flow which are lower in white than gray matter (Helenius et al., 2003). Furthermore, BOLD signal is posited to arise from metabolic demand associated with generating post-synaptic potentials, which occurs in largely in gray matter (Logothetis, Pauls, Augath, Trinath, & Oeltermann, 2001). As a consequence of the preceding, it has been accepted that functional imaging of white matter using BOLD fMRI is not probable, and successful reports are likely to be partial volume effects. This is reflected in the disparity of studies targeting gray matter since the inception of fMRI techniques in the early 1990's (Logothetis & Wandell, 2004; Ogawa et al., 1990).

However, despite these claims, since 2001 there have been increasing reports of WM activation using fMRI ie. (Aramaki, 2005; Chiu, Lin, Chuang, Chen, & Huang, 2001; D'Arcy, Hamilton, Jarmasz, Sullivan, & Stroink, 2006; Omura et al., 2004; Tettamanti et al., 2002; Weber et al., 2005). These reports are commensurate with improvements in both technologies of apparatus and design of sequences yielding increased fMRI signal-to-noise ratio and statistical contrast-to-noise. One of the advances in techniques include high field fMRI (3-4 T vs. 1.5 T), which has proven to be more sensitive to activation in both WM and GM, as well as more specific to WM (Mazerolle et al., 2013). Additionally, new asymmetric spiral sequences have been proven to be most effective, achieving WM activation in up to 100% of individuals (Gawryluk, Brewer, Beyea, & D'Arcy, 2009; Mazerolle et al., 2010).

One potential confounding factor in WM fMRI is the models used to process the experimental data. According to a study by Tae et al, while investigating brain function in an auditory task, it was postulated that WM regions including the corpus callosum could have up to 8 seconds of blood flow increase onset lag beyond the canonical HRF (Tae, Yakunina, Kim, Kim, & Nam, 2014). Due to the nature of GLM analysis, any systematic difference between physiological and modelled form of hemodynamic response would result in reduced assignment of statistical activation. However, a contrasting study using finite impulse response analysis of WM fMRI signal reported the HRF's of GM and WM were of similar form, but WM exhibited reduced amplitude (Fraser, Stevens, Beyea, & D'Arcy, 2012).

The direction since these initial reports has been to determine methods in which activation can be reliably driven, and reject the null hypothesis of interpreting WM activity as artifact. Many of these studies are discussed at length in a recent review (Gawryluk et al., 2014). The primary target WM structures for observing activation in these studies are the corpus callosum and internal capsule (eg. Fabri, 2014; Gawryluk, D'Arcy, Mazerolle, Brewer, & Beyea, 2011; Polonara et al., 2015). These major thoroughfares of the brain pro-

vide interhemispheric communication and cortex-spinal tract sensory motor communication respectively (Kandel & Schwartz, 2012). With prior knowledge of the functional roles of these structures, experimental paradigms, such as the Sperry task, using interhemispheric transfer of information as well as motor responses have been developed with the specific goal of generating activity in WM to be observed using functional imaging (D'Arcy et al., 2006).

Despite the evidence, some research groups still use white matter activity as the baseline threshold of fMRI activity, (eg. Xu et al., 2015). However, others have begun to treat activation on a network level, allowing for the inclusion of white matter while investigating neurological correlates of motor speech learning (Segawa, Tourville, Beal, & Guenther, 2015). Furthermore, structural and functional imaging using MR have been used to identify connectivity pathways in the language network (Vassal et al., 2016).

Based upon the positive foundation of WM fMRI results, non-invasive studies are being performed to understand the regionally specific function of highly connected hubs in the brain, notably the corpus callosum. Topological mapping of corpus callosum has been carried out using a collection of different tasks involving various sensory, motor, and cognitive correlates (Fabri, 2014; Fabri, Polonara, Mascioli, Salvolini, & Manzoni, 2011; Polonara et al., 2015). Using the Sperry and Poffenberger paradigms, reliable activation was localized to specific segments along the corpus callosum (Gawryluk, D'Arcy, et al., 2011). It has also been shown that functional connectivity between hemispheres was recruited more strongly during more difficult tasks (Davis, Cabeza, Davis, & Cabeza, 2015).

A method of reaffirming the positive results of WM fMRI is the inclusion of DTI tractography. This technique involves using the principle components of diffusion tensors to construct probabilistic pathways of white matter tracts. Clusters of fMRI activation can be cross referenced for connectivity. Co-localization within the anisotropic structure of WM is additional evidence against WM fMRI activation being a partial volume effect. It is evident that the addition of DTI for WM activity is advantageous. Methods postulated by Raz & Levin in cases of dysfunction of the visual pathway are discussed in the context of using DTI weighted fMRI to elucidate a better understanding of the clinical condition (Raz & Levin, 2014). Additionally, there is evidence to suggest that fractional anisotropy correlates to task performance indicating another link between structure and function of white matter integrity (Yamamoto et al., 2015). The relationship between structure and function remains widely studied by many types of medical imaging (Garcés et al., 2016).

Chapter 2

Confirmation of WM activity in fMRI using conventional GRE EPI sequences at 3 T

2.1 Background

Nearly half of the brain is white matter, which is comprised of the axons connecting different gray matter regions of the brain's complete network. White matter is involved in the pathology of several debilitating conditions such as multiple sclerosis and dementia (eg. Kim et al., 2015; Paul, 2016). The ability to measure white matter functional activity in healthy and diseased conditions may provide insight leading to new clinical avenues for the treatment or management of such disorders. A focus of neuroimaging research is understanding distributed functional networks in the both healthy control and patient populations.

Most functional magnetic resonance imaging (fMRI) research focuses on gray matter (GM) functional mapping and connectivity. These studies are conducted under the assumption that signals in white matter are physiologically below the threshold required to generate an detectable blood oxygenation level dependent (BOLD) contract response in fMRI (Logothetis & Wandell, 2004). While white matter fMRI detection has since been reported, the degree to which it is commonly observed remains in question partially because the successful reports of WM fMRI have originated from using highly specialized methods (Gawryluk et al., 2014; Fabri, 2014). Additionally, WM activity has shown decreased MR signal amplitude compared to that of GM (Logothetis & Wandell, 2004; Mazerolle et al., 2010; Tettamanti et al., 2002). This is due in part to reduced blood flow and volume in WM as compared to GM, as well as the hemodynamic response being driven primarily by the metabolic demand of the post-synaptic potentials that are thought to be localized in

the GM (Helenius et al., 2003; Logothetis et al., 2001; Preibisch & Haase, 2001; Rostrup et al., 2000; van der Zande, Hofman, & Backes, 2005).

White matter-focused fMRI studies to-date have been done using tasks designed to drive interhemispheric transfer such as visual and motor tasks. These tasks are used to elicit activation in the corpus callosum and internal capsule at both the individual and group levels as illustrated in Figure 2.1, (eg. Gawryluk, D'Arcy, et al., 2011; Gawryluk, Mazerolle, Brewer, Beyea, & D'Arcy, 2011). Many of the studies reporting WM fMRI activity have employed highly specialized methods including the use of high-field MRI, specialized pulse sequences, and advanced analyses techniques (Brewer, Rioux, D'Arcy, Bowen, & Beyea, 2009; Mazerolle et al., 2013). For instance, Brewer et al. used an asymmetric spin-echo (ASE) sequence that allowed for a combination of three spiral acquisitions per volume to increase SNR and CNR. An additional advantage of ASE sequences was that it allows contrast of likeness to combinations of SE and GRE, and for increased sensitivity to field perturbations such as the kind measured in blood oxygenation level dependent (BOLD) fMRI (Stables, Kennan, & Gore, 1998). Due in part to their modern and complex nature, ASE sequences of the kind used by Brewer et al. have not been readily available in all MRI systems, which could have impact on their lack of use in fMRI studies. Similarly, coregistration of fMRI and seeded tractography showed that functionally active regions in white matter are structurally connected to GM regions (Mazerolle et al., 2010). Recently, groups dedicated to developing a functional map of the corpus callosum have used fMRI, DTI, and time course analysis data to show corpus callosum activation in task specific regions using difference sensory stimuli (Fabri et al., 2011; Gawryluk, D'Arcy, et al., 2011; Polonara et al., 2015).

Functional MRI depends on hemodynamic response; however, it remains unclear as to whether or not white matter regions possess a different hemodynamic response as compared to gray matter. There are reports indicating the response will be of the same form, but with reduced amplitude (Fraser et al., 2012), while others postulate a delayed response and lower amplitude (Tae et al., 2014). Understanding the physiological basis of fMRI response in white matter will guide signal interpretation to be more sensitive to brain activity in a regionally specific manner, and would likely increase the prevalence of positively reported activity in future studies. If there are differences in white matter and gray matter hemodynamic responses, analysis protocols that depend on a hemodynamic response function (HRF) convolution are currently optimized for gray matter. Optimization for a potential white matter HRF could significantly enhance sensitivity for white matter fMRI activation.

The aim of the current study was to assess the feasibility of WM fMRI detection using clinically available equipment without technical access or modification to the hardware or sequences. Our objectives were to 1) assess the robustness and utility of clinical WM fMRI using a visual-motor interhemispheric transfer paradigm and 2) to compare activity in the posterior corpus callosum and internal capsule with previous work which implemented

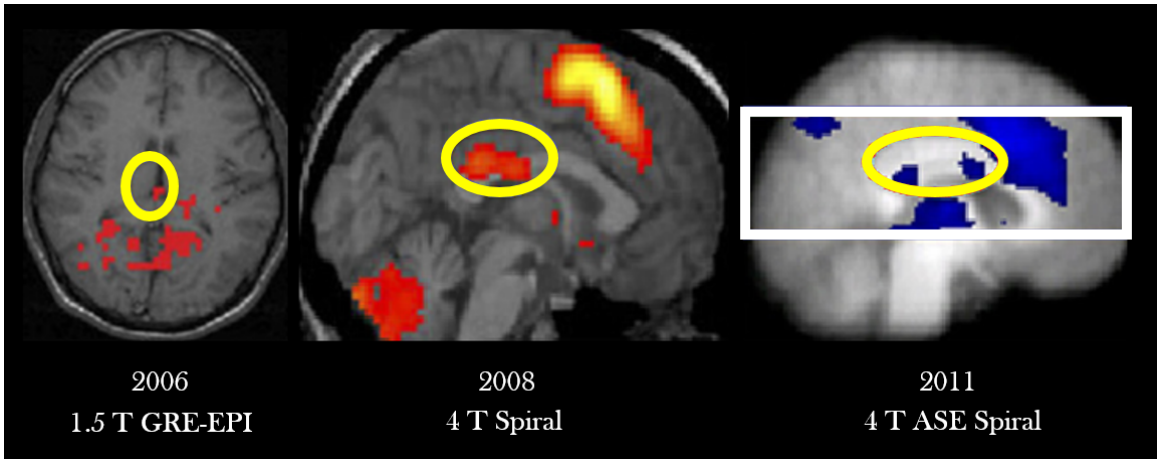

Figure 2.1: Summary of results from previous studies WM fMRI studies, with corpus callosum activation clusters circled in yellow. 2006 (Left): The first report of WM fMRI from this group, the Sperry task, a 1.5 T scanner, and GRE-EPI sequence followed by exploratory analysis were employed (D'Arcy et al., 2006). 2008 (Center): Using improved apparatus including a 4 T scanner, a multi-shot spiral sequence (Mazerolle et al., 2008). 2011 (Right): Optimized ASE spiral sequences scanning a reduced FOV (white box) (Gawryluk, D'Arcy, et al., 2011).

customized sequences on a 4 T MRI (eg. Gawryluk, D'Arcy, et al., 2011; Mazerolle et al., 2010), and 3) to probe for regional effects of analysis model on functional activation sensitivity.

2.2 Methods

2.2.1 Participants

This study was approved by the research ethics boards of Simon Fraser University, the University of British Columbia, and Fraser Health Authority. Fourteen healthy, right handed subjects (seven females) participated in the study. The mean age of participant was 24.4±2.4 years, (range 20-29 years). The mean level of education of participant was 4.17±1.03 years post-secondary. Each participant received an explanation of the study and gave written informed consent prior to participation and received compensation.

2.2.2 Experimental design

Participants performed an interhemispheric transfer task, known as the Sperry task (D'Arcy et al., 2006) to stimulate motor cross and visual-motor cross conditions. A fixation "+" was present for the duration of the experiment to maintain eye position. Right or left hemisphere lateralized stimuli were presented in the form of four-letter vertical words or pseudowords, faces, or pseudo faces (rearranged eyes, nose, mouth) projected briefly in

the left or right visual hemifield, greater than 2.3° from center fixation to prevent overlap (Presentation 15.0, Neurobehavioral Systems, Berkeley, USA). Stimuli were presented for 150 ms to reduce saccades (Gezeck, Fischer, & Timmer, 1997), with an interstimulus interval jittered 2-4 s in blocks of eight, totaling 22 s on, with 18 s rest between blocks. Participants were asked to respond via button response boxes, using left or right index or middle finger to classify the stimulus as word, pseudoword, face, or pseudo face as quickly as possible. Practice blocks were presented prior to experiment to improve compliance and accuracy. The experiments were presented in two halves in randomized order. The dexterity of face and word responses were switched in the second half.

2.2.3 MRI acquisition

MRI data were acquired using a 3.0 T Philips Achieva whole body MRI system, at the UBC MRI Research Centre. An 8-channel Philips SENSE head coil was used.

Functional MRI

Functional MRI data were captured using a Philips FFE single-shot GRE-EPI sequence. Thirty-five (3 mm thick, no gap) transverse slices were collected in interleaved order, with a 3 mm x 3 mm in-plane resolution for a total field of view of 288 mm RL x 288 mm AP x 139 mm FH. The parameters for functional imaging were as follows: TE = 30 ms, flip angle = 90°, TR = 2000 ms. The scan volume was oriented to cover the entire brain.

Structural MRI

A 3D T1-weighted sequence was used to capture structural images and used for co-registration of functional images. One hundred and ninety contiguous 1 mm slices were collected, with a 1 mm x 1 mm in-plane resolution for a total field of view of 256 mm AP x 256 mm FH x 190 mm RL. The sequence parameters were as follows: TE = 3.7 ms, flip angle = 8°, TR = 8.1 ms.

2.2.4 Functional MRI analysis

T_2^*-weighted fMRI data were analyzed using FMRIB Software Library 5.0.9 (FSL) (Jenkinson et al., 2012). Data were initially explored using MELODIC 3.14 for removal of artifacts and physiological noise (Beckmann & Smith, 2005). Pre-statistic processing was performed in FEAT 6.0, and included steps of motion correction with MCFLIRT, brain extraction with BET, spatially smoothing with a Gaussian filter of kernel 5 mm FWHM, and temporally high pass filtered at 80 s. Statistical analyses were carried out using a generalized linear model. The data were pre-whitened using FILM. Predictors were constructed using a double-gamma HRF as well as HRF0, HRF1, HRF2, and HRF3 generated from FLOBS. (Table 2.1, Figure 2.2). Cluster corrected thresholding was applied at $Z > 2.3$ and $Z > 2.0$

with P = 0.05. Individual functional statistics were registered within FEAT to respective T_1-weighted structural images and MNI152 standard space using FLIRT and FNIRT (Jenkinson & Smith, 2001). Registrations to structural and standard spaces were manually verified and corrected as needed.

Model	M1 (s)	M2 (s)	M3 (s)	M4 (s)	c	Bases
HRF0	0-2	3-8	3-8	3-8	0-0.3	3
HRF1	0-3	3-10	3-5	3-8	0-0.3	3
HRF2	0-4	3-12	3-5	3-5	0-0.3	3
HRF3	0-5	3-14	3-4	3-4	0-0.3	3

Table 2.1: FLOBS parameters for generating hemodynamic response function bases. HRF0 represents the FSL defaults HRF0, and HRF1-3 are modified with a longer ramp up time to account for a delayed hemodynamic response in WM as postulated by Tae (Tae et al., 2014).

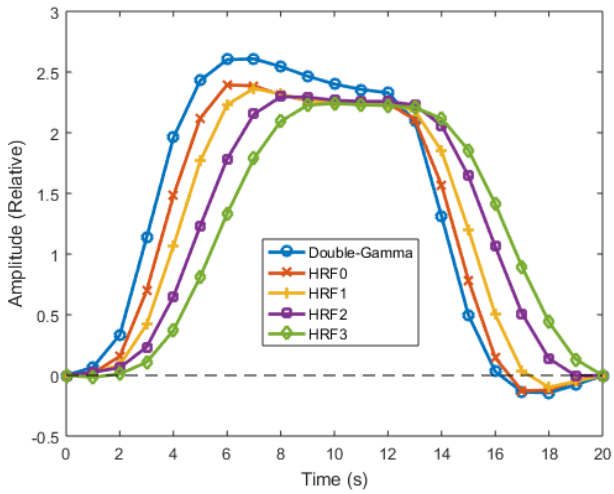

Figure 2.2: HRFs generated using FLOBS. The successive HRFs are characterized by a decreased onset slope and reduced initial overshoot.

After first level analyses, two the half-runs for each individual were combined using FEAT higher-level analysis with fixed effects. Individual Z-statistic images were generated from the resulting combined data, reporting task versus rest contrast. These results were assessed for associated GM function corresponding to the task, as well as activation within the WM of the corpus callosum and internal capsule.

Group level analyses were conducted using FEAT higher-level analysis with FLAME1 mixed effects. Group Z-statistic images were generated from task versus rest contrast. Group level results were investigated in the aforementioned WM and GM regions of interest (ROI) using Featquery. Region of interest masks of the colossal body, internal capsule (corticospinal tract), primary motor cortex, and supplementary motor area were generated

from the Jülich Histological atlas (Amunts, Malikovic, Mohlberg, Schormann, & Zilles, 2000; Burgel, Schormann, Schleicher, & Zilles, 1999; Bürgel et al., 2006; Geyer, 2004; Geyer et al., 1996). ROI mask of the cerebellum was generated from the MNI Structural Atlas (Mazziotta et al., 2001). Probability of thresholds of 50% or greater were used for the WM structures to reduce partial volume contamination between ROI's, and a 10% greater for GM structures. Additionally, any overlap of WM ROI's with the masks of GM were removed in favor of GM.

2.3 Results

2.3.1 Task compliance

A single participant was excluded from analysis due to improper task responses. Comparable to prior studies, the remaining 13 participants completed the tasks with a mean accuracy of 84.13±0.02 % across all targets, and a reaction time of 640±70 ms.

2.3.2 Group-level results

Whole brain analysis at the group level indicated activation consistent with recognizing words and faces and providing motor responses in the Sperry task, at typical thresholds of $Z > 2.3$. GM activity is present in the cerebellum, superior and lateral occipital cortices, temporooccipital fusiform, inferior frontal gyrus, motor and premotor cortices Figure 2.3. These GM results are consistent with previous studies using the Sperry task (Mazerolle et al., 2008).

Group level white matter activation in corpus callosum was found only in the analysis using $Z > 2.0$ thresholding, with a peak Z score of 2.568. Activation was localized to the same anterior mid-body corpus callosum region as previously reported Figure 2.4 (Gawryluk, D'Arcy, et al., 2011). In the $Z > 2.3$ threshold, only two voxels were found to be active within the corpus callosum ROI. Full details of group ROI results are found in Table 2.2.

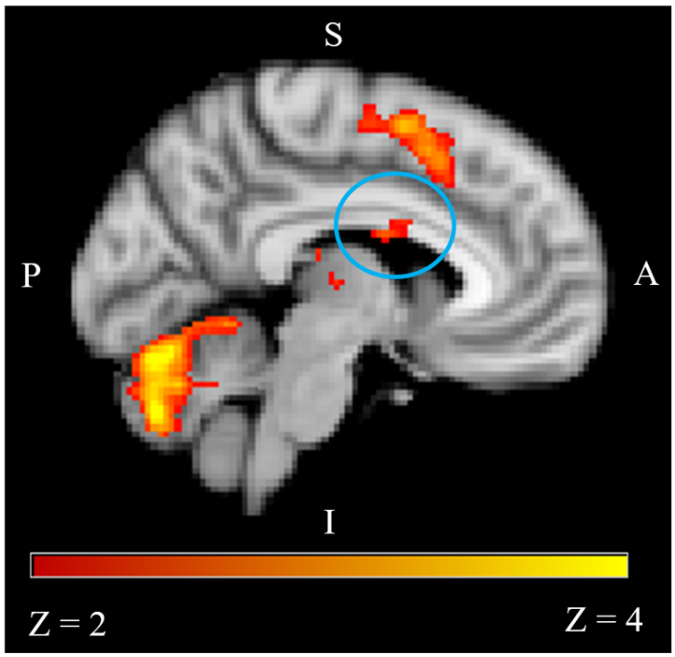

Figure 2.3: Group level summary from HRF1 with threshold Z > 2.0. Corpus callosum activity circled in blue. GM activity in the supplementary motor area and cerebellum are present, in agreement with the nature of the task.

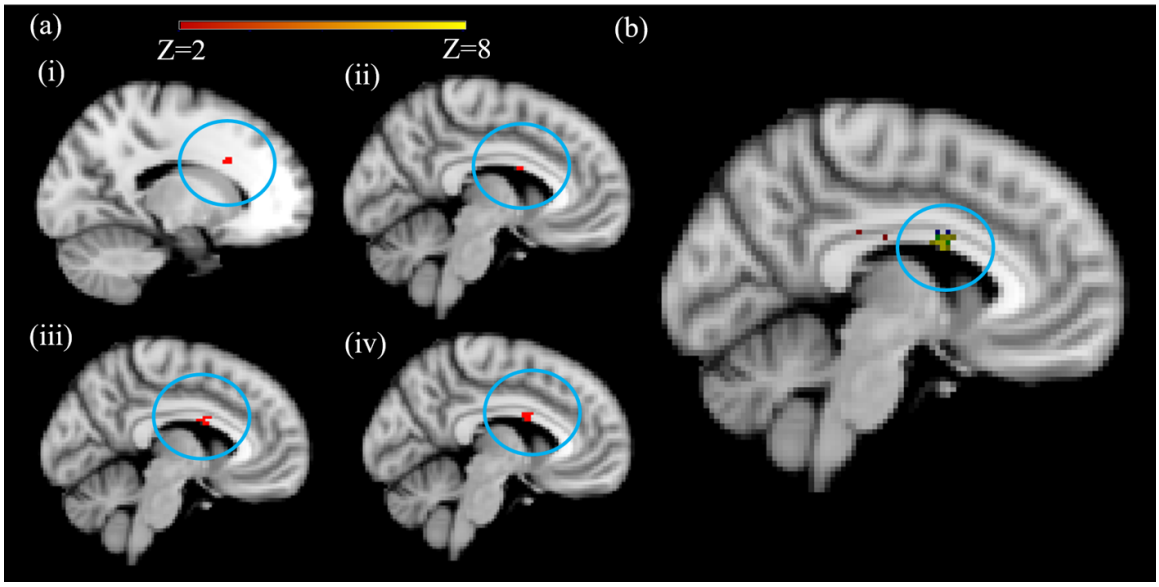

Figure 2.4: HRF dependent group level activation: (a): Group results from analysis using model (i) DG-HRF, (ii) HRF0, (iii) HRF1, (iv) HRF0. CC activity circled in blue. (b): Superposition of the four HRF's Red: DG-HRF, Blue: HRF0, Green: HRF1, and Yellow: HRF2

The standard double-gamma HRF, followed by the FLOBS default HRF0, provided the most sensitivity in almost all regions, with the exception of the corpus callosum. In these regions, sensitivity and Z scores decreased with the sequential shift in onset time of the successive HRF's. Analyses using HRF1 and HRF2 provided superior sensitivity and comparable Z scores in the corpus callosum when compared to the typical HRF's. HRF3 returned no active clusters at the group level. Full details of group ROI survey of the varied HRF's are found in Table 2.2.

ROI	*Model*	$N(Z > 2.0)$	$N(Z > 2.3)$	Z_{max}	x (mm)	y (mm)	z (mm)
CC	DG	8	2	2.568	-14	-32	28
	HRF0	7	0	2.222	-6	2	22
	HRF1	18	0	2.336	-6	4	26
	HRF2	14	0	2.365	-6	2	24
PMC	DG	722	502	4.353	-40	-32	50
	HRF0	554	374	3.960	-56	4	26
	HRF1	360	201	3.639	-56	4	26
	HRF2	66	16	2.647	-38	-34	50
SMA	DG	4801	3770	5.143	4	14	56
	HRF0	4117	3057	4.814	4	14	56
	HRF1	3155	2223	4.486	4	14	56
	HRF2	1063	364	3.559	6	28	50
Cerebellum	DG	6837	5892	5.781	32	-58	-26
	HRF0	6389	5448	5.552	32	-58	-26
	HRF1	5665	4842	5.321	32	-58	-26
	HRF2	4159	3205	4.669	32	-60	-24

Table 2.2: Group ROI results. Number of active voxels contained within the respective ROI at Z > 2.0 and Z > 2.3 Cluster corrected with P = 0.05. Z_{max} are the peak Z scores within the ROI, with location specified in MNI coordinates. In all cases except the corpus callosum, double-gamma and canonical HRF0 provided the most activation, with number of above-threshold voxels and Z scores decreasing with increasing latency of HRF. HRF3 omitted due to eliciting no above-threshold activation the regions.

2.3.3 Individual-level results

Of the 13 individuals analyzed, eight indicated some activation in the corpus callosum (61.5 %) when using the conventional double-gamma HRF and thresholds of Z > 2.3. Figure 2.5 shows the corpus callosum activation of the eight individuals. The average maximum Z score within active individuals in the corpus callosum was 4.58 (SD = 1.07). Additionally, Table 2.3 provides the percent signal change peaks within the WM ROI for all individuals. Individuals with activity in the corpus callosum had a mean percent signal

change of 0.968 (SD = 0.445) and the remainder had a mean of 0.432 (SD = 0.248). Using a t-test, the difference between these groups is significant ($p < 0.05$).

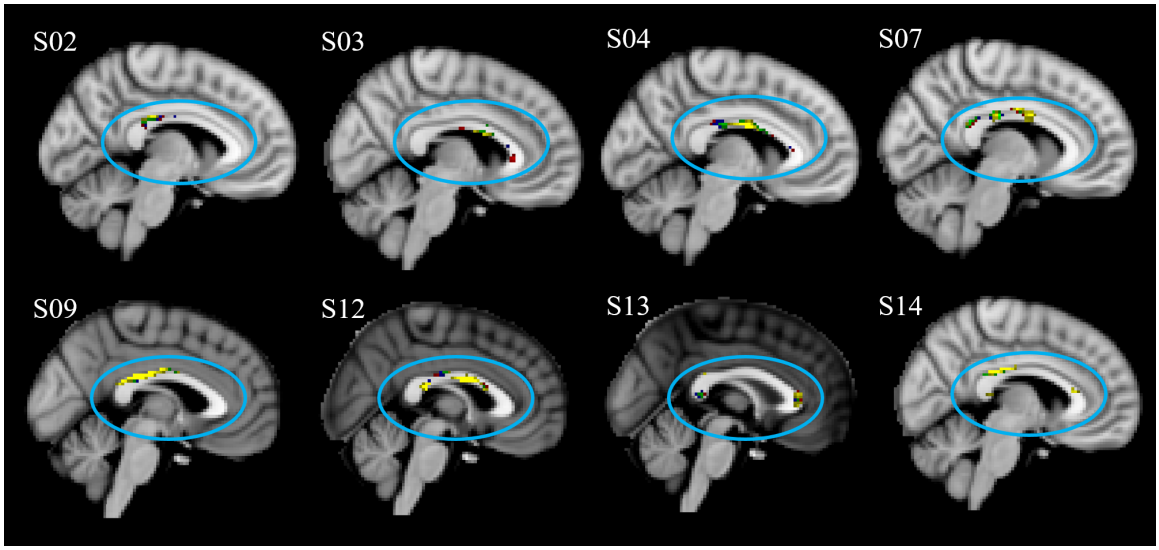

Figure 2.5: Individual level activation, CC circled in blue. Superposition of the four HRF's Red: DG-HRF, Blue: HRF0, Green: HRF1, and Yellow: HRF2.

ID	PSC_{max} (%)	x (mm)	y (mm)	z (mm)
1	.3489	8	-30	28
2	0.3173	0	-22	24
3	1.085	4	4	20
4	1.022	4	8	18
5	0.2668	-20	-16	36
7	0.8614	-4	2	24
8	0.8673	-6	2	22
9	1.399	-2	-30	26
10	0.2494	0	0	28
11	0.3496	-2	4	20
12	1.709	6	2	22
13	0.5576	0	-38	8
14	0.7900	16	30	2

Table 2.3: Percent signal change peaks for all subjects within corpus callosum ROI. Individuals shaded in gray showed above-threshold activation within the respective ROI. A significant difference exists between the mean PSC difference between the active and not-active groups in the CC ($p > 0.05$). Participant 6 absent due to data being excluded from analysis

2.4 Discussion

The Sperry task is design to elicit bilateral activation in the parietal, frontal, cingulate, fusiform and cerebellar regions, as well as interhemispheric transfer within the posterior portions of the corpus callosum, and the motor pathway via the internal capsule (D'Arcy et al., 2006; Gawryluk, D'Arcy, et al., 2011). In the current study, localization of activation in GM is consistent with task design and previous reports using similar paradigms. In the current study, activity in the white matter was investigated using an interhemispheric transfer task. At the group level, activation was distributed bilaterally between the frontal, parietal, as well as the body of the corpus callosum, and the internal capsule. Individual level representation at 61.5 % is weaker than the 100 % reported when using asymmetric spiral sequences (Gawryluk, D'Arcy, et al., 2011), but more successful than earlier studies, also using 4 T conventional spirals, (eg. Mazerolle et al., 2008). In addition, the group level localization in the anterior midbody of the corpus callosum is consistent with the same previous studies, as well as existing functional maps of the corpus callosum (eg. Fabri et al., 2011).

While the predicted white matter fMRI clusters were confirmed in this study, they were notably weaker in extent than have been previously reported. In the individuals showing CC activation, the mean percent signal change of 0.968 detected using 3 T GRE-EPI is consistent with that previously reported using 4 T ASE spiral (Mazerolle et al., 2010). This, combined with the significantly lower percent signal change in the non-active group is consistent with the previously reported individual variability in strength of activation that requireeds highly sensitive methods to detect reliably at the individual level. Individual variance in this study is likely accounted for by both the reduction in field strength and the conventional fMRI pulse sequence used in the present study design. Importantly, these factors may help to explain the historically controversial differences in detecting white matter fMRI activity.

By varying the hemodynamic response function used in the general linear model analysis, it is evident that sensitivity to activation in white matter was dependent on the specific form of the function used. Conflicting reports of the existence of a WM specific HRF have cited physiological (Tae et al., 2014), or empirical fMRI evidence (Fraser et al., 2012) for and against, respectively. When decreasing the onset slope of the HRF, all GM regions showed decreased sensitivity in above-threshold count, as well as Z score maxima. However, HRF's with a delayed waveform yielded a larger above threshold voxel count, and consistent Z maximum in the corpus callosum. Each HRF provided shifted clusters, indicating that local variations likely exist in hemodynamics of white matter, which may be tied to perfusion. The result of the HRF analyses does not necessarily agree the findings of either Tae or Fraser, however in future experiments a multi-model approach may be ideal to increase sensitivity to activation in physiologically varied regions of the brain. Furthermore, it should be noted

that most of the white matter fMRI experiments performed have used the same paradigms with similar block timings (eg. Fraser et al., 2012; Gawryluk, D'Arcy, et al., 2011). If WM exhibits an extended hemodynamic response time than GM, experiments designed to have longer blocks may allow the BOLD signal to reach a higher peak amplitude in regions of less perfusion.

Limitations of this study include the relatively small sample size. While this will have likely impacted statistical power at the group-level analysis and sensitivity at the individual-level analysis, prior published work has used comparable sample sizes enabling the balanced comparison. In ROI analyses, partial volumes remain an issue when using probabilistic masks, and when localizing fMRI results at the individual- or group-level using spatial smoothing and registration transforms. The true resolution of functional data remains diffuse leading to potential false-negative results in successive stages of statistical analysis. In this study statistical thresholds of $Z > 2.0$ cluster corrected, $P = 0.05$ were employed in order to elicit above-threshold activity in WM, as has been done previously (Gawryluk, D'Arcy, et al., 2011). The small effect size under conventional experimental conditions of WM fMRI remains a challenge to its credibility in the neuroimaging community (Logothetis & Wandell, 2004).

As MRI technology continues to be developed, its power to resolve indistinct phenomena will grow. One of the most recent advances in parallelized MR technology is simultaneous multi-slice acquisition using multiband excitation (Moeller et al., 2010). This revelation allows for an increase in both temporal and spatial resolution while reducing acquisition time for structural images (Feinberg & Setsompop, 2013). High-rate fMRI measurements could increase SNR of measurement yielding more reliable statistical results as well as a more detailed observation of observable phenomena such as hemodynamic response.

Chapter 3

Conclusion

3.1 Functional MRI in white matter

Most of the pioneering studies in WM fMRI employed specialized and advanced methodology including 4 T scanners, specialized pulse sequences, and advanced analysis methods. These sequences are custom programmed by researchers on their specific hardware and other groups may not be able replicate the experiments without great investment, leading to dubiousness. We replicated white matter fMRI activation in the corpus callosum using standard 3 T MRI and GRE-EPI fMRI. By showing corpus callosum activation at the group level, and at 61.5% on the individual level using clinically accessible methods reinforces that white matter fMRI observations are nonspurious. However, this study indicates that for future research in distributed networks, WM BOLD signal is detectable using clinically accessible methods, but requires focused protocols. High percentage individual detection is presently best accomplished with higher field scanners and modified spiral sequences. In future, applying optimized spiral sequences, with multiband excitation, along with direct physiological multi modal measures including magnetoencephalography may yield suitably robust activation in WM functional detection at the individual level providing a foothold for clinical utility.

3.2 Significance

The capability for reliable, individual white matter functional methods will be beneficial towards the following aims:

1. In the healthy brain: fMRI will be able to functionally observe the more of the dynamic connectivity making up the human connectome. This will provide greater insight into the modular computing nature of the brain.

2. In plasticity: white matter function is able to drive structural changes, which may be observed using fMRI.

3. In disease: improved capability to diagnose, monitor, and understand several clinical conditions involving white matter integrity changes, including AD, MS, dementia, etc..

3.3 Future research directions

3.3.1 In magnetic resonance imaging

In this experiment, there was no optimization of sequence parameters in MR acquisition. Larger sample testing between different sequences and sequence parameters such as echo time may elucidate optimal experimental conditions. Ideal experimental methods such as specialized pulse sequences and higher field magnets may not be practically accessible to all studies. However, improvements in analysis methods including updated software libraries are widely available and beneficial to many researchers. In order to have a greater understanding of the hemodynamic response of various brain regions, use finite impulse response analysis to survey the brain. Knowing spatial dependence of this metabolic response, construct a regional atlas of HRF's which can provide more accurate statistical analyses for functional measures with mechanisms based on blood flow. With a more accurate model for every tissue, functional activation will resolve with greater statistical confidence.

In addition to modeling the hemodynamic response in all tissues, functional studies using longer active block designs should be used to allow BOLD signal saturation. If BOLD signal has differential onset slope across tissues, allowing for saturated activation will detect changes in slower regions. Additionally, when analyzing a saturated signal, the onset dynamics can be compared with greater confidence due to the defined separation between ramp-up and ramp-down.

While BOLD is the dominant mechanism used in fMRI research, others such as SEEP have been underutilized. BOLD is a method which is linked to metabolic processes driving blood flow, whereas SEEP relies solely on extracellular water movement. SEEP was developed to work in spinal cord fMRI. In white matter tissue with markedly less cerebral blood flow and volume, a non-blood dependent contrast mechanism may prove to be an effective tool.

3.3.2 In magnetoencephalography

Magnetoencephalography (MEG) is a medical imaging system in which femtotesla magnetic fields generated by neuronal currents are measured in order to observe the functional dynamics of the human brain. Current strategies in MEG data analysis focus on localizing electro-physiological sources within a shallow region below the surface of cortical gray matter of the brain, leaving the connected network structure of deep brain white matter. Conducting action potetials generate magnetic fields in white matter, and exhibit a quadrupolar

nature in contrast to gray matter dipoles. These sources propagate along a trajectory defined by the structural connectivity of the brain, which can be volumetrically charted using diffusion-weighted magnetic resonance imaging. Given that magnetoencephalograpy systems of varying sensor array designs can measure deeper brain signals, the aim of my future research is to develop computational tools, including a conductivity-based head model and quadrupolar source reconstruction algorithm, to enable observation of real-time functional activity in the white matter. Not only would MEG detection of WM functional activation provide further evidence for the validity of fMRI results, it also allows for much higher temporal resolution observation of brain connectivity.

1. From a MEG technical perspective, it has been shown that the complexity of head model provided stronger source localization when considering external factors such as WM anisotropy and cerebrospinal fluid (Vorwerk et al., 2014). A realistic conductivity-based model would provide a more complete picture for all MEG localization experiments.

2. A serviceable method to image WM function using MEG in real-time would be complementary to fMRI techniques, and further beneficial to the study, diagnosis, and management of some of white matter diseases.

3. In clinical use, MEG serves epileptic focii localization. Expanding the utility of MEG for research and clinical use in more areas of the brain, for specific disease cases, and for the spinal cord (Adachi et al., 2015) would provide similar growth as seen in MRI research, which has had a large impact in both research and diagnostic medicine.

References

Adachi, Y., Kawabata, S., Sasano, T., Oyama, Y. H. D., Uehara, G., & Sekihara, K. (2015). Biomagnetic measurement system for supine subjects with expanded sensor array and real-time noise reduction. In *Annu. int. conf. ieee eng. med. biol. soc.* (Vol. 2015, pp. 7071–4). Retrieved from http://www.ncbi.nlm.nih.gov/pubmed/26737921 doi: 10.1109/EMBC.2015.7320021

Alhilali, L. M., Delic, J. A., Gumus, S., & Fakhran, S. (2015, dec). Evaluation of White Matter Injury Patterns Underlying Neuropsychiatric Symptoms after Mild Traumatic Brain Injury. *Radiology*, *277*(3), 793–800. Retrieved from http://pubs.rsna.org/doi/10.1148/radiol.2015142974 doi: 10.1148/radiol.2015142974

Amunts, K., Malikovic, A., Mohlberg, H., Schormann, T., & Zilles, K. (2000, jan). Brodmann's Areas 17 and 18 Brought into Stereotaxic SpaceâĂŤWhere and How Variable? *Neuroimage*, *11*(1), 66–84. Retrieved from http://linkinghub.elsevier.com/retrieve/pii/S1053811999905165 doi: 10.1006/nimg.1999.0516

Aramaki, Y. (2005, nov). Neural Correlates of the Spontaneous Phase Transition during Bimanual Coordination. *Cereb. Cortex*, *16*(9), 1338–1348. Retrieved from http://www.ncbi.nlm.nih.gov/pubmed/16306323http://www.cercor.oxfordjournals.org/cgi/doi/10.1093/cercor/bhj075 doi: 10.1093/cercor/bhj075

Armstrong, R. A. (2010). A quantitative study of the pathological changes in the cortical white matter in variant Creutzfeldt-Jakob disease (vCJD). *Clin. Neuropathol.*, *29*(6), 390–6. Retrieved from http://www.ncbi.nlm.nih.gov/pubmed/21073844

Armstrong, R. C., Mierzwa, A. J., Marion, C. M., & Sullivan, G. M. (2016, jan). White matter involvement after TBI: Clues to axon and myelin repair capacity. *Exp. Neurol.*, *275 Pt 3*, 328–33. Retrieved from http://www.ncbi.nlm.nih.gov/pubmed/25697845 doi: 10.1016/j.expneurol.2015.02.011

Astafiev, S. V., Shulman, G. L., Metcalf, N. V., Rengachary, J., MacDonald, C. L., Harrington, D. L., ... Corbetta, M. (2015, aug). Abnormal White Matter Blood-Oxygen-LevelâĂŞDependent Signals in Chronic Mild Traumatic Brain Injury. *J. Neurotrauma*, *32*(16), 1254–1271. Retrieved from http://www.ncbi.nlm.nih.gov/pubmed/25758167http://online.liebertpub.com/doi/10.1089/neu.2014.3547 doi: 10.1089/neu.2014.3547

Beckmann, C., & Smith, S. (2005, mar). Tensorial extensions of independent component analysis for multisubject FMRI analysis. *Neuroimage*, *25*(1), 294–311. Retrieved from http://linkinghub.elsevier.com/retrieve/pii/S1053811904006378 doi: 10.1016/j.neuroimage.2004.10.043

Bengtsson, S. L., Nagy, Z., Skare, S., Forsman, L., Forssberg, H., & Ullén, F. (2005, sep). Extensive piano practicing has regionally specific effects on white matter development. *Nat. Neurosci.*, *8*(9), 1148–1150. Retrieved from http://www.nature.com/doifinder/10.1038/nn1516 doi: 10.1038/nn1516

Black, S. E. (2007, mar). Imaging white matter and the burden of small vessel disease. *Brain Cogn.*, *63*(2), 192–193. Retrieved from http://www.sciencedirect.com/science/article/pii/S0278262606002193http://linkinghub.elsevier.com/retrieve/pii/S0278262606002193 doi: 10.1016/j.bandc.2006.08.010

Bloch, F. (1946, oct). Nuclear Induction. *Phys. Rev.*, *70*(7-8), 460–474. Retrieved from http://link.aps.org/doi/10.1103/PhysRev.70.460 doi: 10.1103/PhysRev.70.460

Bogen, J. E., & Vogel, P. J. (1962). Cerebral commissurotomy in man. *Bull Los Angeles Neurol Soc*, *27*(4), 169–172.

Brewer, K. D., Rioux, J. a., D'Arcy, R. C. N., Bowen, C. V., & Beyea, S. D. (2009, jul). Asymmetric spin-echo (ASE) spiral improves BOLD fMRI in inhomogeneous regions. *NMR Biomed.*, *22*(6), 654–662. Retrieved from http://www.ncbi.nlm.nih.gov/pubmed/19382109http://doi.wiley.com/10.1002/nbm.1380 doi: 10.1002/nbm.1380

Bugiani, M., Boor, I., Powers, J. M., Scheper, G. C., & van der Knaap, M. S. (2010, oct). Leukoencephalopathy With Vanishing White Matter: A Review. *J. Neuropathol. Exp. Neurol.*, *69*(10), 987–996. Retrieved from http://jnen.oxfordjournals.org/lookup/doi/10.1097/NEN.0b013e3181f2eafa doi: 10.1097/NEN.0b013e3181f2eafa

Bürgel, U., Amunts, K., Hoemke, L., Mohlberg, H., Gilsbach, J. M., & Zilles, K. (2006, feb). White matter fiber tracts of the human brain: Three-dimensional mapping at microscopic resolution, topography and intersubject variability. *Neuroimage*, *29*(4), 1092–1105. Retrieved from http://linkinghub.elsevier.com/retrieve/pii/S105381190500649X doi: 10.1016/j.neuroimage.2005.08.040

Burgel, U., Schormann, T., Schleicher, A., & Zilles, K. (1999, nov). Mapping of histologically identified long fiber tracts in human cerebral hemispheres to the MRI volume of a reference brain: position and spatial variability of the optic radiation. *Neuroimage*, *10*(5), 489–499. doi: 10.1006/nimg.1999.0497

Buxton, R. B., Wong, E. C., & Frank, L. R. (1998, jun). Dynamics of blood flow and oxygenation changes during brain activation: the balloon model. *Magn. Reson. Med.*, *39*(6), 855–64. Retrieved from http://www.ncbi.nlm.nih.gov/pubmed/9621908

Caprihan, A., Jones, T., Chen, H., Lemke, N., Abbott, C., Qualls, C., ... Bustillo, J. R. (2015, aug). The Paradoxical Relationship between White Matter, Psychopathology and Cognition in Schizophrenia: A Diffusion Tensor and Proton Spectroscopic Imaging Study. *Neuropsychopharmacology*, *40*(9), 2248–2257. Retrieved from http://www.nature.com/doifinder/10.1038/npp.2015.72 doi: 10.1038/npp.2015.72

Caverzasi, E., Mandelli, M. L., DeArmond, S. J., Hess, C. P., Vitali, P., Papinutto, N., ... Henry, R. G. (2014, dec). White matter involvement in sporadic Creutzfeldt-Jakob disease. *Brain*, *137*(Pt 12), 3339–3354. doi: 10.1093/brain/awu298

Chiu, M., Lin, C., Chuang, K., Chen, J., & Huang, K. (2001, mar). Tissue segmentation-assisted analysis of fMRI for human motor response: an approach combining artificial neural network and fuzzy C means. *J. Digit. Imaging*, *14*(1), 38–47. Retrieved from http://link.springer.com/10.1007/s10278-001-0023-y doi: 10.1007/s10278-001-0023-y

D'Arcy, R. C. N., Hamilton, A., Jarmasz, M., Sullivan, S., & Stroink, G. (2006, apr). Exploratory data analysis reveals visuovisual interhemispheric transfer in functional magnetic resonance imaging. *Magn. Reson. Med.*, *55*(4), 952–8. Retrieved from http://www.ncbi.nlm.nih.gov/pubmed/16506159 doi: 10.1002/mrm.20839

D'Arcy, R. C. N., Lindsay, D. S., Song, X., Gawryluk, J. R., Greene, D., Mayo, C., ... Greene, T. (2015, sep). Long-Term Motor Recovery After Severe Traumatic Brain Injury. *J. Head Trauma Rehabil.*, *31*(5),

E50–E58. Retrieved from http://content.wkhealth.com/linkback/openurl?sid=WKPTLP:landingpage{&}an=00001199-900000000-99674http://www.ncbi.nlm.nih.gov/pubmed/26360005http://content.wkhealth.com/linkback/openurl?sid=WKPTLP:landingpage{&}an=00001199-201609000-00013 doi: 10.1097/HTR.0000000000000185

Davis, X. S. W., Cabeza, R., Davis, S. W., & Cabeza, R. (2015). Cross-Hemispheric Collaboration and Segregation Associated with Task Difficulty as Revealed by Structural and Functional Connectivity. *J. Neurosci.*, *35*(21), 8191–8200. doi: 10.1523/JNEUROSCI.0464-15.2015

Dawe, R. J., Yu, L., Leurgans, S. E., Schneider, J. A., Buchman, A. S., Arfanakis, K., ... Boyle, P. A. (2016, sep). Postmortem MRI: a novel window into the neurobiology of late life cognitive decline. *Neurobiol. Aging*, *45*, 169–177. Retrieved from http://linkinghub.elsevier.com/retrieve/pii/S0197458016300926 doi: 10.1016/j.neurobiolaging.2016.05.023

Douek, P., Turner, R., Pekar, J., Patronas, N., & Le Bihan, D. (1991). MR color mapping of myelin fiber orientation. *J. Comput. Assist. Tomogr.*, *15*(6), 923–9. Retrieved from http://www.ncbi.nlm.nih.gov/pubmed/1939769

Droby, A., Yuen, K. S. L., Muthuraman, M., Reitz, S.-C., Fleischer, V., Klein, J., ... Groppa, S. (2015, nov). Changes in brain functional connectivity patterns are driven by an individual lesion in MS: a resting-state fMRI study. *Brain Imaging Behav.*. Retrieved from http://link.springer.com/10.1007/s11682-015-9476-3 doi: 10.1007/s11682-015-9476-3

Evans, A. C., Collins, D. L., Mills, S. R., Brown, E. D., Kelly, R. L., & Peters, T. M. (1993, oct). 3D statistical neuroanatomical models from 305 MRI volumes. In *Nucl. sci. symp. med. imaging conf. 1993., 1993 ieee conf. rec.* (pp. 1813–1817 vol.3). doi: 10.1109/NSSMIC.1993.373602

Fabri, M. (2014). Functional topography of the corpus callosum investigated by DTI and fMRI. *World J. Radiol.*, *6*(12), 895. Retrieved from http://www.embase.com/search/results?subaction=viewrecord{&}from=export{&}id=L70363373{%}5Cnhttp://sfx.library.uu.nl/utrecht?sid=EMBASE{&}issn=19714009{&}id=doi:{&}atitle=Functional+topography+of+the+corpus+callosum+as+depicted+by+fMRI+and+DTI+investigations{&}stitle=N doi: 10.4329/wjr.v6.i12.895

Fabri, M., Polonara, G., Mascioli, G., Salvolini, U., & Manzoni, T. (2011, jan). Topographical organization of human corpus callosum: an fMRI mapping study. *Brain Res.*, *1370*, 99–111. Retrieved from http://dx.doi.org/10.1016/j.brainres.2010.11.039http://www.ncbi.nlm.nih.gov/pubmed/21081115 doi: 10.1016/j.brainres.2010.11.039

Feinberg, D. A., & Setsompop, K. (2013, apr). Ultra-fast MRI of the human brain with simultaneous multi-slice imaging. *J. Magn. Reson.*, *229*, 90–100. Retrieved from http://www.ncbi.nlm.nih.gov/pmc/articles/PMC3793016/http://linkinghub.elsevier.com/retrieve/pii/S1090780713000311 doi: 10.1016/j.jmr.2013.02.002

Figley, C. R., Leitch, J. K., & Stroman, P. W. (2010, oct). In contrast to BOLD: signal enhancement by extravascular water protons as an alternative mechanism of endogenous fMRI signal change. *Magn. Reson. Imaging*, *28*(8), 1234–43. Retrieved from http://www.ncbi.nlm.nih.gov/pubmed/20299173 doi: 10.1016/j.mri.2010.01.005

Filley, C. M., & Fields, R. D. (2016, nov). White matter and cognition: making the connection. *J. Neurophysiol.*, *116*(5), 2093–2104. Retrieved from http://jn.physiology.org/lookup/doi/10.1152/jn.00221.2016 doi: 10.1152/jn.00221.2016

Fraser, L. M., Stevens, M. T., Beyea, S. D., & D'Arcy, R. C. N. (2012, jan). White versus gray matter: fMRI hemodynamic responses show similar characteristics, but differ in peak amplitude. *BMC Neurosci.*, *13*(1), 91. Retrieved from http://www.pubmedcentral.nih.gov/articlerender.fcgi?artid=3469381{&}tool=pmcentrez{&}rendertype=abstract doi: 10.1186/1471-2202-13-91

Garcés, P., Pereda, E., Hernández-Tamames, J. A., Del-Pozo, F., Maestú, F., & Ángel Pineda-Pardo, J. (2016, jan). Multimodal description of whole brain connectivity: A comparison of resting state MEG, fMRI, and DWI. *Hum. Brain Mapp.*, *37*(1), 20–34. Retrieved from http://doi.wiley.com/10.1002/hbm.22995http://www.ncbi.nlm.nih.gov/pubmed/26503502 doi: 10.1002/hbm.22995

Gawryluk, J. R., Brewer, K. D., Beyea, S. D., & D'Arcy, R. C. (2009, mar). Optimizing the detection of white matter fMRI using asymmetric spin echo spiral. *Neuroimage*, *45*(1), 83–88. Retrieved from http://www.ncbi.nlm.nih.gov/pubmed/19084071http://linkinghub.elsevier.com/retrieve/pii/S105381190801210X doi: 10.1016/j.neuroimage.2008.11.005

Gawryluk, J. R., D'Arcy, R. C., Mazerolle, E. L., Brewer, K. D., & Beyea, S. D. (2011, jan). Functional mapping in the corpus callosum: A 4T fMRI study of white matter. *Neuroimage*, *54*(1), 10–15. Retrieved from http://www.sciencedirect.com/science/article/B6WNP-50JHBVM-4/2/c1b59cfb4cf77b714bda3d4498519feb{%}5Cnhttp://www.ncbi.nlm.nih.gov/pubmed/20643213http://linkinghub.elsevier.com/retrieve/pii/S1053811910010013 doi: 10.1016/j.neuroimage.2010.07.028

Gawryluk, J. R., Mazerolle, E. L., Brewer, K. D., Beyea, S. D., & D'Arcy, R. C. N. (2011, jan). Investigation of fMRI activation in the internal capsule. *BMC Neurosci.*, *12*(1), 56. Retrieved from http://www.pubmedcentral.nih.gov/articlerender.fcgi?artid=3141570{&}tool=pmcentrez{&}rendertype=abstract doi: 10.1186/1471-2202-12-56

Gawryluk, J. R., Mazerolle, E. L., & D'Arcy, R. C. N. (2014, jan). Does functional MRI detect activation in white matter? A review of emerging evidence, issues, and future directions. *Front. Neurosci.*, *8*(August), 239. Retrieved from http://www.pubmedcentral.nih.gov/articlerender.fcgi?artid=4125856{&}tool=pmcentrez{&}rendertype=abstracthttp://www.ncbi.nlm.nih.gov/pubmed/25152709http://www.pubmedcentral.nih.gov/articlerender.fcgi?artid=PMC4125856 doi: 10.3389/fnins.2014.00239

Gazzaniga, M. S., Bogen, J. E., & Sperry, R. W. (1965, jun). Observations on visual perception after disconnexion of the cerebral hemispheres in man. *Brain*, *88*(2), 221–36. Retrieved from http://brain.oxfordjournals.org/content/88/2/221.abstracthttp://www.ncbi.nlm.nih.gov/pubmed/5828904

Geschwind, N. (1965, jun). Disconnexion syndromes in animals and man. I. *Brain*, *88*(2), 237–94. Retrieved from http://brain.oxfordjournals.org/content/88/2/237.abstracthttp://brain.oxfordjournals.org/content/88/3/585.abstracthttp://www.ncbi.nlm.nih.gov/pubmed/5318481

Geyer, S. (2004). The microstructural border between the motor and the cognitive domain in the human cerebral cortex. *Adv. Anat. Embryol. Cell Biol.*, *174*, I–VIII, 1–89. Retrieved from http://www.ncbi.nlm.nih.gov/pubmed/14750415

Geyer, S., Ledberg, A., Schleicher, A., Kinomura, S., Schormann, T., Burgel, U., ... Roland, P. E. (1996, aug). Two different areas within the primary motor cortex of man. *Nature*, *382*(6594), 805–807. Retrieved from http://dx.doi.org/10.1038/382805a0

Gezeck, S., Fischer, B., & Timmer, J. (1997, aug). Saccadic reaction times: a statistical analysis of multimodal distributions. *Vision Res.*, *37*(15), 2119–2131. Retrieved from http://www.sciencedirect.com/science/article/pii/S0042698997000229 doi: http://dx.doi.org/10.1016/S0042-6989(97)00022-9

Giedd, J. N. (2004, jun). Structural magnetic resonance imaging of the adolescent brain. *Ann. N. Y. Acad. Sci.*, *1021*, 77–85. Retrieved from http://www.ncbi.nlm.nih.gov/pubmed/15251877 doi: 10.1196/annals.1308.009

Gordon, B. A., Najmi, S., Hsu, P., Roe, C. M., Morris, J. C., & Benzinger, T. L. (2015). The effects of white matter hyperintensities and amyloid deposition on Alzheimer dementia. *NeuroImage Clin.*, *8*, 246–252. Retrieved from http://linkinghub.elsevier.com/retrieve/pii/S2213158215000844 doi: 10.1016/j.nicl.2015.04.017

Graveline, C. J., Mikulis, D. J., Crawley, A. P., & Hwang, P. A. (1998, nov). Regionalized sensorimotor plasticity after hemispherectomy fMRI evaluation. *Pediatr. Neurol.*, *19*(5), 337–342. Retrieved from http://www.ncbi.nlm.nih.gov/pubmed/9880136http://linkinghub.elsevier.com/retrieve/pii/S0887899498000824 doi: 10.1016/S0887-8994(98)00082-4

Habes, M., Erus, G., Toledo, J. B., Zhang, T., Bryan, N., Launer, L. J., ... Davatzikos, C. (2016, apr). White matter hyperintensities and imaging patterns of brain ageing in the general population. *Brain*, *139*(Pt 4), 1164–1179. doi: 10.1093/brain/aww008

Hajnal, J. V., Doran, M., Hall, A. S., Collins, A. G., Oatridge, A., Pennock, J. M., ... Bydder, G. M. (1991). MR imaging of anisotropically restricted diffusion of water in the nervous system: technical, anatomic, and pathologic considerations. *J. Comput. Assist. Tomogr.*, *15*(1), 1–18. Retrieved from http://www.ncbi.nlm.nih.gov/pubmed/1987175

He, Y., & Evans, A. (2010, jun). Graph theoretical modeling of brain connectivity. *Curr. Opin. Neurol.*, *23*(4), 1. Retrieved from http://content.wkhealth.com/linkback/openurl?sid=WKPTLP:landingpage{&}an=00019052-900000000-99865 doi: 10.1097/WCO.0b013e32833aa567

Heggdal, P. O. L., Brännström, J., Aarstad, H. J., Vassbotn, F. S., & Specht, K. (2016, feb). Functional-structural reorganisation of the neuronal network for auditory perception in subjects with unilateral hearing loss: Review of neuroimaging studies. *Hear. Res.*, *332*, 73–79. Retrieved from http://linkinghub.elsevier.com/retrieve/pii/S0378595515300083 doi: 10.1016/j.heares.2015.11.015

Helenius, J., Perkiö, J., Soinne, L., Østergaard, L., Carano, R. a. D., Salonen, O., ... Tatlisumak, T. (2003, jan). Cerebral Hemodynamics in a Healthy Population Measured by Dynamic Susceptibility Contrast Mr Imaging. *Acta radiol.*, *44*(5), 538–546. Retrieved from http://www.ncbi.nlm.nih.gov/pubmed/14510762http://acr.sagepub.com/lookup/doi/10.1080/j.1600-0455.2003.00104.x doi: 10.1080/j.1600-0455.2003.00104.x

ITU-R. (2015). *Recommendation V.431: Standard Letter Designations for Radar-Frequency Bands.*

Jäncke, L., Gaab, N., Wüstenberg, T., Scheich, H., & Heinze, H. J. (2001, dec). Short-term functional plasticity in the human auditory cortex: an fMRI study. *Brain Res. Cogn. Brain Res.*, *12*(3), 479–85. Retrieved from http://www.ncbi.nlm.nih.gov/pubmed/11689309 doi: 10.1016/S0926-6410(01)00092-1

Jenkinson, M., Beckmann, C. F., Behrens, T. E., Woolrich, M. W., & Smith, S. M. (2012, aug). FSL. *Neuroimage*, *62*(2), 782–790. Retrieved from http://linkinghub.elsevier.com/retrieve/pii/S1053811911010603 doi: 10.1016/j.neuroimage.2011.09.015

Jenkinson, M., & Smith, S. M. (2001). A global optimization method for robust affine registration of brain images. *Med. Imaging Anal.*, *5*, 143–156.

Jochimsen, T. H., Norris, D. G., & Möller, H. E. (2005, feb). Is there a change in water proton density associated with functional magnetic resonance imaging? *Magn. Reson. Med.*, *53*(2), 470–473. Retrieved from http://dx.doi.org/10.1002/mrm.20351 doi: 10.1002/mrm.20351

Jung, W.-B., Mun, C.-W., Kim, Y.-H., Park, J. M., Lee, B. D., Lee, Y. M., ... Chung, Y. I. (2014, dec). Cortical atrophy, reduced integrity of white matter and cognitive impairment in subcortical vascular dementia of Binswanger type. *Psychiatry Clin. Neurosci.*, *68*(12), 821–832. Retrieved from http://doi.wiley.com/10.1111/pcn.12196 doi: 10.1111/pcn.12196

Kandel, E. R., & Schwartz, J. H. (2012). *Principles of Neural Science* (Fifth ed.; T. M. Jessell, S. A. Siegelbaum, & A. Hudspeth, Eds.). McGraw-Hill. Retrieved from http://www.amazon.com/Principles-Neural-Science-Eric-Kandel/dp/0071120009

Kim, S., Choi, S. H., Lee, Y. M., Kim, M. J., Kim, Y. D., Kim, J. Y., ... Kim, D. K. (2015, dec). Periventricular white matter hyperintensities and the risk of dementia: a CREDOS study. *Int. Psychogeriatrics*, *27*(12), 2069–2077. Retrieved from http://www.journals.cambridge.org/abstract{_}S1041610215001076 doi: 10.1017/S1041610215001076

Larkman, D. J., Hajnal, J. V., Herlihy, A. H., Coutts, G. A., Young, I. R., & Ehnholm, G. (2001, feb). Use of multicoil arrays for separation of signal from multiple slices simultaneously excited. *J. Magn. Reson. Imaging*, *13*(2), 313–7. Retrieved from http://www.ncbi.nlm.nih.gov/pubmed/11169840

Larmor, J. (1897, dec). LXIII. On the theory of the magnetic influence on spectra; and on the radiation from moving ions. *Philos. Mag. Ser. 5*, *44*(271), 503–512. Retrieved from http://dx.doi.org/10.1080/14786449708621095http://www.tandfonline.com/doi/abs/10.1080/14786449708621095 doi: 10.1080/14786449708621095

Lassmann, H. (2014, nov). Mechanisms of white matter damage in multiple sclerosis. *Glia*, *62*(11), 1816–30. Retrieved from http://www.ncbi.nlm.nih.gov/pubmed/24470325 doi: 10.1002/glia.22597

Lee, H., Cohen, O. S., Rosenmann, H., Hoffmann, C., Kingsley, P. B., Korczyn, A. D., ... Prohovnik, I. (2012, nov). Cerebral White Matter Disruption in Creutzfeldt-Jakob Disease. *Am. J. Neuroradiol.*, *33*(10), 1945–1950. Retrieved from http://www.ajnr.org/cgi/doi/10.3174/ajnr.A3125 doi: 10.3174/ajnr.A3125

Logothetis, N. K., Pauls, J., Augath, M., Trinath, T., & Oeltermann, a. (2001). Neurophysiological investigation of the basis of the fMRI signal. *Nature*, *412*(6843), 150–157. doi: 10.1038/35084005

Logothetis, N. K., & Wandell, B. a. (2004, mar). Interpreting the BOLD Signal. *Annu. Rev. Physiol.*, *66*(1), 735–769. Retrieved from http://www.ncbi.nlm.nih.gov/pubmed/14977420http://www.annualreviews.org/doi/10.1146/annurev.physiol.66.082602.092845 doi: 10.1146/annurev.physiol.66.082602.092845

Love, S., & Miners, J. S. (2015, jan). White Matter Hypoperfusion and Damage in Dementia: Post-Mortem Assessment. *Brain Pathol.*, *25*(1), 99–107. Retrieved from http://www.ncbi.nlm.nih.gov/pubmed/25521180http://doi.wiley.com/10.1111/bpa.12223 doi: 10.1111/bpa.12223

Mahoney, C. J., Ridgway, G. R., Malone, I. B., Downey, L. E., Beck, J., Kinnunen, K. M., ... Warren, J. D. (2014, aug). Profiles of white matter tract pathology in frontotemporal dementia. *Hum. Brain Mapp.*, *35*(8), 4163–4179. doi: 10.1002/hbm.22468

Marzi, C. a., Perani, D., Tassinari, G., Colleluori, A., Maravita, A., Miniussi, C., ... Fazio, F. (1999, jun). Pathways of interhemispheric transfer in normals and in a split-brain subject. *Exp. Brain Res.*, *126*(4), 451–458. Retrieved from http://www.ncbi.nlm.nih.gov/pubmed/10422707http://link.springer.com/10.1007/s002210050752 doi: 10.1007/s002210050752

Matsusue, E., Kinoshita, T., Sugihara, S., Fujii, S., Ogawa, T., & Ohama, E. (2004). White matter lesions in panencephalopathic type of Creutzfeldt-Jakob disease: MR imaging and pathologic correlations. *Am. J. Neuroradiol.*, *25*(6), 910–918.

Mazerolle, E. L., Beyea, S. D., Gawryluk, J. R., Brewer, K. D., Bowen, C. V., & D'Arcy, R. C. (2010, apr). Confirming white matter fMRI activation in the corpus callosum: Co-localization with DTI tractography. *Neuroimage*, *50*(2), 616–621. Retrieved from http://www.ncbi.nlm.nih.gov/pubmed/20053383http://linkinghub.elsevier.com/retrieve/pii/S1053811909013913 doi: 10.1016/j.neuroimage.2009.12.102

Mazerolle, E. L., D'Arcy, R. C. N., & Beyea, S. D. (2008, sep). Detecting functional magnetic resonance imaging activation in white matter: interhemispheric transfer across the corpus callosum. *BMC Neurosci.*, *9*, 84. Retrieved from http://www.pubmedcentral.nih.gov/articlerender.fcgi?artid=2553800{&}tool=pmcentrez{&}rendertype=abstracthttp://www.ncbi.nlm.nih.gov/pubmed/18789154http://www.pubmedcentral.nih.gov/articlerender.fcgi?artid=PMC2553800 doi: 10.1186/1471-2202-9-84

Mazerolle, E. L., Gawryluk, J. R., Dillen, K. N. H., Patterson, S. a., Feindel, K. W., Beyea, S. D., ... D'Arcy, R. C. (2013, mar). Sensitivity to White Matter fMRI Activation Increases with Field Strength. *PLoS One*, *8*(3), e58130. Retrieved from http://www.pubmedcentral.nih.gov/articlerender.fcgi?artid=3587428{&}tool=pmcentrez{&}rendertype=abstracthttp://dx.plos.org/10.1371/journal.pone.0058130 doi: 10.1371/journal.pone.0058130

Mazziotta, J., Toga, A., Evans, A., Fox, P., Lancaster, J., Zilles, K., ... Mazoyer, B. (2001, aug). A probabilistic atlas and reference system for the human brain: International Consortium for Brain Mapping (ICBM). *Philos. Trans. R. Soc. B Biol. Sci.*, *356*(1412), 1293–1322. Retrieved from http://www.ncbi.nlm.nih.gov/pmc/articles/PMC1088516/http://rstb.royalsocietypublishing.org/cgi/doi/10.1098/rstb.2001.0915 doi: 10.1098/rstb.2001.0915

McKeown, M. J., Makeig, S., Brown, G. G., Jung, T. P., Kindermann, S. S., Bell, A. J., & Sejnowski, T. J. (1998). Analysis of fMRI data by blind separation into independent spatial components. *Hum. Brain Mapp.*, *6*(3), 160–188.

Meijboom, R., Steketee, R. M. E., de Koning, I., Osse, R. J., Jiskoot, L. C., de Jong, F. J., ... Smits, M. (2016, jul). Functional connectivity and microstructural white matter changes in phenocopy frontotemporal dementia. *Eur. Radiol.*. Retrieved from http://link.springer.com/10.1007/s00330-016-4490-4 doi: 10.1007/s00330-016-4490-4

Menon, R. S., Ogawa, S., Tank, D. W., & Ugurbil, K. (1993, sep). Tesla gradient recalled echo characteristics of photic stimulation-induced signal changes in the human primary visual cortex. *Magn. Reson. Med.*, *30*(3), 380–6. Retrieved from http://www.ncbi.nlm.nih.gov/pubmed/8412612

Moeller, S., Yacoub, E., Olman, C. A., Auerbach, E., Strupp, J., Harel, N., & UÄ§urbil, K. (2010, may). Multiband multislice GE-EPI at 7 tesla, with 16-fold acceleration using partial parallel imaging with application to high spatial and temporal whole-brain fMRI. *Magn. Reson. Med.*, *63*(5), 1144–1153. Retrieved from http://www.ncbi.nlm.nih.gov/pmc/articles/PMC2906244/http://doi.wiley.com/10.1002/mrm.22361 doi: 10.1002/mrm.22361

Moseley, M. E., Cohen, Y., Kucharczyk, J., Mintorovitch, J., Asgari, H. S., Wendland, M. F., ... Norman, D. (1990, aug). Diffusion-weighted MR imaging of anisotropic water diffusion in cat central nervous system. *Radiology*, *176*(2), 439–445. Retrieved from http://www.ncbi.nlm.nih.gov/pubmed/2367658http://pubs.rsna.org/doi/10.1148/radiology.176.2.2367658 doi: 10.1148/radiology.176.2.2367658

Ogawa, S., Lee, T. M., Kay, A. R., & Tank, D. W. (1990, dec). Brain magnetic resonance imaging with contrast dependent on blood oxygenation. *Proc. Natl. Acad. Sci.*, *87*(24), 9868–9872. Retrieved from http://www.pnas.org/content/87/24/9868.shorthttp://www.pubmedcentral.nih.gov/articlerender.fcgi?artid=1262394{&}tool=pmcentrez{&}rendertype=abstract{%}5Cnhttp://www.pnas.org/content/87/24/9868.shorthttp://www.pnas.org/cgi/doi/10.1073/pnas.87.24.9868 doi: 10.1073/pnas.87.24.9868

Omura, K., Tsukamoto, T., Kotani, Y., Ohgami, Y., Minami, M., & Inoue, Y. (2004, dec). Different mechanisms involved in interhemispheric transfer of visuomotor information. *Neuroreport*, *15*(18), 2707–11. Retrieved from http://www.ncbi.nlm.nih.gov/pubmed/15597039

Paul, F. (2016, sep). Pathology and MRI: exploring cognitive impairment in MS. *Acta Neurol. Scand.*, *134*, 24–33. Retrieved from http://www.ncbi.nlm.nih.gov/pubmed/27580903http://doi.wiley.com/10.1111/ane.12649 doi: 10.1111/ane.12649

Polonara, G., Mascioli, G., Foschi, N., Salvolini, U., Pierpaoli, C., Manzoni, T., ... Barbaresi, P. (2015, may). Further Evidence for the Topography and Connectivity of the Corpus Callosum: An fMRI Study of Patients with Partial Callosal Resection. *J. Neuroimaging*, *25*(3), 465–473. Retrieved from http://doi.wiley.com/10.1111/jon.12136 doi: 10.1111/jon.12136

Preibisch, C., & Haase, A. (2001, jul). Perfusion imaging using spin-labeling methods: contrast-to-noise comparison in functional MRI applications. *Magn. Reson. Med.*, *46*(1), 172–82. Retrieved from http://onlinelibrary.wiley.com/doi/10.1002/mrm.1173/fullhttp://www.ncbi.nlm.nih.gov/pubmed/11443724

Pronk, J. C., van Kollenburg, B., Scheper, G. C., & van der Knaap, M. S. (2006). Vanishing white matter disease: A review with focus on its genetics. *Ment. Retard. Dev. Disabil. Res. Rev.*, *12*(2), 123–128. Retrieved from http://doi.wiley.com/10.1002/mrdd.20104 doi: 10.1002/mrdd.20104

Raz, N., & Levin, N. (2014). Cortical and white matter mapping in the visual system-more than meets the eye: on the importance of functional imaging to understand visual system pathologies. *Front. Integr. Neurosci.*, *8*(August), 68. Retrieved from http://www.pubmedcentral.nih.gov/articlerender.fcgi?artid=4145715{&}tool=pmcentrez{&}rendertype=abstracthttp://www.ncbi.nlm.nih.gov/pubmed/25221482http://www.pubmedcentral.nih.gov/articlerender.fcgi?artid=PMC4145715 doi: 10.3389/fnint.2014.00068

Rostrup, E., Law, I., Blinkenberg, M., Larsson, H., Born, A., Holm, S., & Paulson, O. (2000, feb). Regional Differences in the CBF and BOLD Responses to Hypercapnia: A Combined PET and fMRI Study. *Neuroimage*, *11*(2), 87–97. Retrieved from http://www.ncbi.nlm.nih.gov/pubmed/10679182http://linkinghub.elsevier.com/retrieve/pii/S1053811999905268 doi: 10.1006/nimg.1999.0526

Scholz, J., Klein, M. C., Behrens, T. E. J., & Johansen-Berg, H. (2009, nov). Training induces changes in white-matter architecture. *Nat. Neurosci.*, *12*(11), 1370–1371. Retrieved from http://www.nature.com/doifinder/10.1038/nn.2412 doi: 10.1038/nn.2412

Sedaghat, S., Cremers, L. G. M., de Groot, M., Hofman, A., van der Lugt, A., Niessen, W. J., ... Vernooij, M. W. (2016, aug). Lower microstructural integrity of brain white matter is related to higher mortality. *Neurology*, *87*(9), 927–934. doi: 10.1212/WNL.0000000000003032

Segawa, J. A., Tourville, J. A., Beal, D. S., & Guenther, F. H. (2015, apr). The Neural Correlates of Speech Motor Sequence Learning. *J. Cogn. Neurosci.*, *27*(4), 819–831. Retrieved from http://www.mitpressjournals.org/doi/abs/10.1162/jocn{_}a{_}00737 doi: 10.1162/jocn_a_00737

Stables, L. A., Kennan, R. P., & Gore, J. C. (1998, sep). Asymmetric spin-echo imaging of magnetically inhomogeneous systems: theory, experiment, and numerical studies. *Magn. Reson. Med.*, *40*(3), 432–442. Retrieved from http://onlinelibrary.wiley.com/doi/10.1002/mrm.1910400314/full

Stejskal, E. O., & Tanner, J. E. (1965). Spin Diffusion Measurements: Spin Echoes in the Presence of a Time-Dependent Field Gradient. *J. Chem. Phys.*, *42*(1), 288. Retrieved from http://scitation.aip.org/content/aip/journal/jcp/42/1/10.1063/1.1695690 doi: 10.1063/1.1695690

Stroman, P., Krause, V., Malisza, K., Frankenstein, U., & Tomanek, B. (2002, jul). Extravascular proton-density changes as a non-BOLD component of contrast in fMRI of the human spinal cord. *Magn. Reson. Med.*, *48*(1), 122–127. Retrieved from http://www.ncbi.nlm.nih.gov/pubmed/12111939http://doi.wiley.com/10.1002/mrm.10178 doi: 10.1002/mrm.10178

Tae, W. S., Yakunina, N., Kim, T. S., Kim, S. S., & Nam, E.-C. (2014, jul). Activation of auditory white matter tracts as revealed by functional magnetic resonance imaging. *Neuroradiology*, *56*(7), 597–605. Retrieved from http://link.springer.com/10.1007/s00234-014-1362-y doi: 10.1007/s00234-014-1362-y

Taylor, A. N., Kambeitz-Ilankovic, L., Gesierich, B., Simon-Vermot, L., Franzmeier, N., Araque Caballero, M. Á., ... Ewers, M. (2016, jul). Tract-specific white matter hy-

perintensities disrupt neural network function in Alzheimer's disease. *Alzheimer's Dement.*. Retrieved from http://www.ncbi.nlm.nih.gov/pubmed/27432800http://linkinghub.elsevier.com/retrieve/pii/S1552526016326607 doi: 10.1016/j.jalz.2016.06.2358

Tettamanti, M., Paulesu, E., Scifo, P., Maravita, A., Fazio, F., Perani, D., & Marzi, C. A. (2002). Interhemispheric transmission of visuomotor information in humans: fMRI evidence. *J. Neurophysiol.*, *88*, 1051–1058. doi: 10.1152/jn.00417.2001

Trojan, S., & Pokorný, J. (1999). Theoretical aspects of neuroplasticity. *Physiol. Res.*, *48*(2), 87–97.

van der Zande, F. H. R., Hofman, P. a. M., & Backes, W. H. (2005, feb). Mapping hypercapnia-induced cerebrovascular reactivity using BOLD MRI. *Neuroradiology*, *47*(2), 114–20. Retrieved from http://www.ncbi.nlm.nih.gov/pubmed/15616848 doi: 10.1007/s00234-004-1274-3

Vassal, F., Schneider, F., Boutet, C., Jean, B., Sontheimer, A., & Lemaire, J.-J. (2016, mar). Combined DTI Tractography and Functional MRI Study of the Language Connectome in Healthy Volunteers: Extensive Mapping of White Matter Fascicles and Cortical Activations. *PLoS One*, *11*(3), e0152614. Retrieved from http://dx.plos.org/10.1371/journal.pone.0152614 doi: 10.1371/journal.pone.0152614

Vorwerk, J., Cho, J.-H., Rampp, S., Hamer, H., Knösche, T. R., & Wolters, C. H. (2014, oct). A guideline for head volume conductor modeling in EEG and MEG. *Neuroimage*, *100*, 590–607. Retrieved from http://dx.doi.org/10.1016/j.neuroimage.2014.06.040http://linkinghub.elsevier.com/retrieve/pii/S1053811914005175 doi: 10.1016/j.neuroimage.2014.06.040

Wang, X.-N., Zeng, Y., Chen, G.-Q., Zhang, Y.-H., Li, X.-Y., Hao, X.-Y., ... Han, Y. (2014, nov). Abnormal organization of white matter networks in patients with subjective cognitive decline and mild cognitive impairment. *Oncotarget*. Retrieved from http://www.oncotarget.com/abstract/10601 doi: 10.18632/oncotarget.10601

Weber, B., Treyer, V., Oberholzer, N., Jaermann, T., Boesiger, P., Brugger, P., ... Marzi, C. A. (2005, jan). Attention and Interhemispheric Transfer: A Behavioral and fMRI Study. *J. Cogn. Neurosci.*, *17*(1), 113–123. Retrieved from http://www.mitpressjournals.org/doi/abs/10.1162/0898929052880002 doi: 10.1162/0898929052880002

Xu, C., Li, C., Wu, H., Wu, Y., Hu, S., Zhu, Y., ... Zhang, X. (2015). Gender Differences in Cerebral Regional Homogeneity of Adult Healthy Volunteers: A Resting-State fMRI Study. *Biomed Res. Int.*, *2015*, 1–8. Retrieved from http://www.hindawi.com/journals/bmri/2015/183074/http://www.ncbi.nlm.nih.gov/pubmed/25629038http://www.pubmedcentral.nih.gov/articlerender.fcgi?artid=PMC4299532https://www.hindawi.com/journals/bmri/2015/183074/ doi: 10.1155/2015/183074

Yamamoto, M., Kushima, I., Kimura, H., Hayashi, A., Kawano, N., Aleksic, B., ... Ozaki, N. (2015, oct). White matter microstructure between the pre-SMA and the cingulum bundle is related to response conflict in healthy subjects. *Brain Behav.*, *5*(10), n/a–n/a. Retrieved from http://www.ncbi.nlm.nih.gov/pubmed/26516610http://www.pubmedcentral.nih.gov/articlerender.fcgi?artid=PMC4614048http://doi.wiley.com/10.1002/brb3.375 doi: 10.1002/brb3.375

Zeeman, P. (1897, feb). The Effect of Magnetisation on the Nature of Light Emitted by a Substance. *Nature*, *55*(1424), 347–347. Retrieved from http://www.nature.com/doifinder/10.1038/055347a0 doi: 10.1038/055347a0

Zhang, X. Y., Fan, F.-M., Chen, D.-C., Tan, Y.-L., Tan, S.-P., Hu, K., ... Soares, J. C. (2016, feb). Extensive White Matter Abnormalities and Clinical Symptoms in Drug-Naive Patients With First-Episode Schizophrenia. *J. Clin. Psychiatry*, *77*(2), 205–211. Retrieved from http://www.psychiatrist.com/jcp/article/pages/2016/v77n02/v77n0213.aspx doi: 10.4088/JCP.14m09374

Zhong, X.-P., Chen, Y.-X., Li, Z.-Y., Shen, Z.-W., Kong, K.-M., & Wu, R.-H. (2016, jun). Cervical spinal functional magnetic resonance imaging of the spinal cord injured patient during electrical stimulation. *Eur. Spine J.*. Retrieved from http://www.ncbi.nlm.nih.gov/pubmed/27311305http://link.springer.com/10.1007/s00586-016-4646-6 doi: 10.1007/s00586-016-4646-6